Master's Thesis
석사 학위논문

A new approach for separation of circulating tumor cells (CTCs) in the microfluidics to enhance the capture purity with COMSOL simulation

Ji Eun Lee (이 지 은 李 智 恩)

Department of Robotics Engineering
로봇공학전공

DGIST

2015

A new approach for separation of circulating tumor cells (CTCs) in the microfluidics to enhance the capture purity with COMSOL simulation

Advisor : Professor SangJun Moon

Co-advisor : Professor Taejoon Park

By

Ji Eun Lee

Department of Robotics Engineering

A thesis submitted to the faculty of DGIST in partial fulfillment of the requirements for the degree of Master of Science in the Department of Robotics Engineering. The study was conducted in accordance with Code of Research Ethics[1]

1.9. 2015

Approved by

Professor SangJun Moon (Signature)
(Advisor)

Professor Taejoon Park (Signature)
(Co-Advisor)

[1] Declaration of Ethical Conduct in Research**:** I, as a graduate student of DGIST, hereby declare that I have not committed any acts that may damage the credibility of my research. These include, but are not limited to: falsification, thesis written by someone else, distortion of research findings or plagiarism. I affirm that my thesis contains honest conclusions based on my own careful research under the guidance of my thesis advisor.

A new approach for separation of circulating tumor cells (CTCs) in the microfluidics to enhance the capture purity with COMSOL simulation

Ji Eun Lee

Accepted in partial fulfillment of the requirements for the degree of Master of Science.

11. 27. 2014

Head of Committee 문 상 준 (인)
Prof. SangJun Moon

Committee Member 박 태 준 (인)
Prof. Taejoon Park

Committee Member 전 원 배 (인)
Dr. Won Bae Jeon

MS/RT

201323010

이 지 은. Ji Eun Lee. A new approach for separation of circulating tumor cells (CTCs) in the microfluidics to enhance the capture purity with COMSOL simulation. Department of Robotics Engineering. 2015. 90p. Advisors Prof. SangJun Moon, Prof. Co-Advisors Taejoon Park.

ABSTRACT

Circulating tumor cells (CTCs) is considered as the indicator of primary cancer of patient since CTCs escape from the primary cancer. The separation and subsequent molecular analysis of CTCs are required to diagnosis, treatment and development of the new drug and biomarker. The microfluidic based separation technology is continuously developed, because of the advantages of microfluidics such as easy handling, low-cost fabrication and integration with optical or electrical systems. The size based hydrodynamic separation technology, especially multi-orifice flow fractionation (MOFF) can offer the high throughout, the high cell viability with labelling process. Also this microfluidic system can isolate CTCs with almost 100% of the capture efficiency, but near to 0% of the capture purity. The problem is the size overlap between a leukocytes and CTCs. The deformability of the cells actually affects to the separation process, however, the deformability of cells is not discussed. To enhance the capture purity, the deformability should be considered, because the cell deformability affects to the result.

In this research, the trajectories of rigid and deformable particles are analyzed using COMSOL simulation. In result, the deformability parameter affects to the change of trajectories of rigid and deformable particles. Moreover the increased fluid velocity and the number of stage enhanced the gap of the trajectories of two types of particles, it should be considered to improve the capture purity as well as the cell size.

Keywords: circulating tumor cells (CTCs), microfluidics, deformability of cell, COMSOL simulation

Contents

List of figures

List of tables

1. Introduction

1.1 Objectives and Motivations

The cancer is known as the diseases group related to an unregulated and excessive growth of cell at any part of body [1]. Formation of new blood or lymphatic vessels called angiogenesis and lymphangiogenesis is a key role of the cancer to steal the oxygen and nutrients from the normal cells and to take these resources, also to excrete waste products for their survival [2, 3]. The cancer having the capability of metastatic property can spread out to near or remote sites and form new tumor mass. The leaved cancer cells from the primary cancer enter to and circulate through the blood vessels or lymphatic streams and then attach to other tissues for a proliferation [2, 3]. Because this cancerous cells can be propagated to almost all of the body, the treatment of the metastatic cancer is harder than the primary cancer. Metastasis is known as the main reason of 90% of the cancer related death [4]. To detect the cancer there are diverse diagnosis methods as a symptoms test, a medical imaging, a tissue and liquid biopsy. The symptoms test that is called the medical interview is the process that the doctor observes the patient and asks detailed questions about the patient's symptoms. During the communication between the doctor and patient, the patient offers his or her suffering symptoms and the history of illness and the doctor catches the nonverbal information as well as the verbal information related to the patient's facial expression, gestures and symptoms of illness [5]. Reiser (1980) claims that regardless of how the physician easily extracts the signs of the patient's illness or the patient explains well about the own symptoms, the guidance and interpersonal skills of the physician are needed to understand and diagnose the patient's disease [5, 6]. Using the medical imaging technologies

such as computed x-ray tomography (CT)[7], magnetic resonance imaging (MRI)[8], and ultrasound (US)[9], the organs suspected cancer or whole body of the patient is scanned to gain the physical properties of the cancer [10]. This medical imaging has been developed for the clear resolution, but it may high-cost method and it may not offer be real-time monitoring [11]. Also the medical imaging may inject the contrast media to enhance the resolution of the imaging for discriminating between the normal and pathological areas, the contrast media has the ability of the adverse effect [12]. The biopsy examines the cancer-derived samples like cancerous tissues or cells, so this method can allow the easy and real-time monitoring of diagnosis and treatment [13]. The tissue biopsy extracts invasively and performs the historical analysis of only a part of organ [14]. Before executing the tissue biopsy the medical imaging is needed to detect to a mass lesion and decided the examination placement of human body [14, 15]. For example, Fine-needle aspiration biopsy (FNAB) [14] is used the small-gauge needle to slightly open the human body and take the assumed tissues [16]. The liquid biopsy is minimally invasive method and detects to the circulating tumor cells (CTCs) that have the genetic information of cancer in the blood. CTCs are the divided cancerous cell from the cancer and circulates through the blood or lymphatic vessels [17]. In comparison to the tissue biopsy, the liquid biopsy examines the blood to detect the CTCs without the medical imaging. Therefore the examination of whole body is impossible so, this method provides more various information about the cancer statement for the diagnosis and treatment of cancer [11, 18-20]. The cancer is diagnosed to more accurate, lower-price and minimal invasive method in real time without the clinical interview and the medical imaging.

CTCs were first described as the small numbers of cells in metastatic cancer patient blood similar to the cells of the initial tumor in 1869 by Thomas Ashworth [21]. CTCs are considered to the seeds for subsequent growth of additional tumors in vital organ and CTCs

trigger the process that is responsible for most cancer-related deaths. In the examination, the detection of CTCs is a basic evidence that the patient get cancer. The advanced care and research would carry out by using CTCs in the clinical field and the cancer study. To use CTCs, it needs not only the separation of CTCs from a complex cell mixture, but also the manipulation the separated alive CTCs for the subsequent analysis [22]. Because the isolation and analysis are processed in regular sequence, a separating CTCs from the derived-blood sample of the patient is an essential procedure.

First, CTCs escape from the primary cancer tissue and this cells directly reflect cancer status in real time [23-26], this cells can be used to understand the cancer status. As an indicator of the cancer, the isolated CTCs from the blood can offer the genetic properties of primary cancer and the physical information like a localization. Therefore the cell and molecular analysis of the separated CTCs from the blood sample can widely be utilized as the companion to the diagnosis, the clinical direction, and the therapy response monitoring of an improvement of the cancer [27]. There is the tumor heterogeneity among various CTC types, between the primary cancer cell and metastatic cell, the same cancer type of different patients, even not the same form of cancer of same patient [11, 28]. The cancer also might acquire the metastatic property in the course of disease progression, also the type of metastasis is different according to cancer type, the patient and the mechanisms drive the formation of metastases [29]. Because the metastasis is significantly related to a mortality, the isolating and identifying of CTCs is the immense clinical importance. Like the saying “If you know your enemy and yourself, you can win every battle”, a knowing about CTCs of the patient is a key procedure for saving the life of patient by the targeted therapy and the analysis result will offer the wider perspective of the alternative cancer state.

Second, CTCs is extremely rare number in the blood from a cancer patient [13, 30, 31],

the enchainment of CTCs by isolating technology is required. In 1 ml of the extracted blood sample, CTCs are found about 1 to 100 cells but the blood cells such as erythrocyte (red blood cell, RBC) and leukocyte (white blood cell, WBC) are estimated ~10^9 and ~10^7 respectively [32, 33]. Despite of CTCs have diverse and direct information of the cancer, the number of CTCs in the blood is very small. CTCs should be maximally or entirely separated from the complex cell mixture and the separated CTCs have to be alive for the subsequent analysis. The characterization of the maximal or entire number of alive CTCs can provide the best exact analysis result [34]. Based on the many information of an enriched CTCs, the proper medical decision and an effective therapy offer to patient with best benefit. Moreover the enrichment of CTCs, which means a pure and complete separation without other cells in the blood, is crucial for the analysis, but the large background of a contamination blood cells still a significant noise to identify the purely separated CTCs [11, 19].

Third, CTCs are used to not only the diagnosis and the therapy, but also the test drug-sensitivity and the development of new drug and biomarker. The other needs of the separation of CTCs is rather than just enumeration of CTCs, it also choose the specific targeted drugs or combination of right drugs for testing the resistance and developing new drugs [35]. The isolated viable CTCs from the blood is used for a biomarker discovery and the development for more useful future clinical applications [36]. The research about new drug and uncovering biomarker are developed based on the characterized CTCs. According to the different cancers and the patients, the therapy method is different and the used drug or biomarker are different. Further, CTCs have various type of the heterogeneity, the development of the proper drug and the discovery of the useful biomarker is needed for the personal treatment and the efficient detection of CTCs.

Greater understating of the cancer mechanisms, heterogeneity, and malignancy can

offer to more exact diagnosis and prognosis to patient, and the individual targeted therapeutic benefit [11, 37-39], moreover the development of new drug and biomarker for the advanced treatment. For these reasons, the improvement of the strategies for the efficient capture, separation and enrichment of CTCs is required for a more accurate identification from the derived blood samples and the advanced medical decision. Moreover an enhanced viability and a pure isolation of CTCs is needed for more precise identification based on the maximum of the purely isolated CTCs.

1.2 Background information

Basically CTCs are physically different from the blood cells such as a leukocyte (white blood cell, WBC) and an erythrocyte (red blood cell, RBC). The physical properties of CTCs are categorized as CTCs have a specific surface molecules and a higher dielectric property than other blood cells, and CTCs are stiffer and larger than other blood cells. Moreover using these physical properties of CTCs, the separation technologies have been introduced and especially the separation has been developed in microfluidic research area [40]. Compared with traditional separation methods, the micro-fabricated device handle small volume of sample and the throughput decreases [41]. Nevertheless the separation technology using the microfluidics can offer many advantages. By the development of the microfluidics , it is possible to handle simultaneously the large number or single of cells in the controlled flow condition and easily integrate to all kinds of analytical system [42, 43]. The microfluidic offer easy and cheap fabrication process and a high-quality replica of microfluidic device [40, 44]. Also on-step sample preparation of the loading-separation-identification, resulting in the reduction of cell loss by the microfluidic system [32].

First, CTCs have the specific surface molecules, which is epithelial cell adhesion molecules (EpCAM) [45]. This epithelial antigen is absent in normal blood cells [46]. Because it only positive to the EpCAM antibody and it is considered a biomarker for the malignant epithelial tumors [47]. The EpCAM and antibody are different according to numerous types of the tumor condition. Using this different antigen-antibody reaction between the normal blood cells and CTCs with EpCAM antibody, CTCs are isolated from the mixture of various cells. After capture process the labelled CTCs with the EpCAM antibody are detected and analyzed by combining with an imaging technology, because of the

fluorescent antibody, which can be stained with fluorescent dye. As shown Fig 1-1., the isolation technologies are developed based on the antigen-antibody reaction. One research group [20], they coated the EpCAM on the micro-posts and the blood sample flows through the microfluidic channel as shown figure 1-1(a). CTCs are bond with antibody and other blood cells pass the antibody trap. Christopher M. Earhart' group [48] used the antibody-conjugated magnetic bead to bind to only CTCs and an applied external magnetic field to separate the CTCs of the lung cancer patient through the magnetic pore structure. This schematic is displayed at figure 1-1(b). The magnetic bead binding with CTCs are isolated by the magnetophoresis and the non-tagging normal blood cells freely flow through the magnetic pore structure. The capture efficiency of high EpCAM expressing cells was greater than 90% and low expressing cells was reduced to 17.7%, respectively [48]. Using the same technology, the commercial system CellSearch® and Anda Test Breast Cancer Select/Detect can isolate CTCs [49]. CellSearch® uses a ferro fluid nanoparticle to bind to CTCs in the diluted blood sample and the antibody on the particle is stained to distinguish CTCs and blood cells [50]. After binding and staining process, the bond CTCs with nanoparticle only are attracted to a magnest in the magnet chamber and then attracted CTCs are scanned by the imaging system. The images show a morphology and the number of captured CTCs, it is not provide the genetic information or analysis results of CTCs. Anda Test Breast Cancer Select/Detect similarly uses the specific magnetic beads, but this beads are coated with Oligo$(dT)_{25}$ to reverse transcription of CTCs after separating process [49]. This system offers the binding process and the separation and cell lysis process to purify the mRNA from CTCs with Oligo$(dT)_{25}$ coated magnetic bead. It also can offer the detection and genetic analysis CTCs by the reverse transcription with extracted mRNA of the separated CTCs. This immunoaffinity method are specifically detect to CTCs, so the sensitivity and septicity are

high. However this method is the labelling method, which labelling decreases the cell viability and disturb the analysis after isolation. After detection and isolation process, the CTCs could not detached resulting in the analysis efficiency decreases [51] and EpCAM expression varies depending on physiological conditions [52]. To overcome these limitations, the negative enrichment separation technology is introduced [52]. Compared with the method that uses coated antibody on the microfluidic channel and detects to CTCs, the negative enrichment method uses geometrically activated surface interaction (GASI) chip [52] the antibody to bind the non-target cells, a leukocyte. When the blood sample flows through the coated antibody on the microfluidic channel, the antibody is positive to the non-target cells and the enrichment of CTCs increases at the output. The capture efficiency was 98.94% and the capture purity was3.64%. Despite of the negative separation technology is the non-labelling method and the capture efficiency was higher than the positive technologies, the blood cells both erythrocytes and leukocytes are extremely larger in number than the number of CTCs in the blood sample, a lot of antibody that can capture the blood cells or CTCs, are needed to enhance the capture purity. The positive and negative enrichment methods need the particular antibody with various type of CTCs.

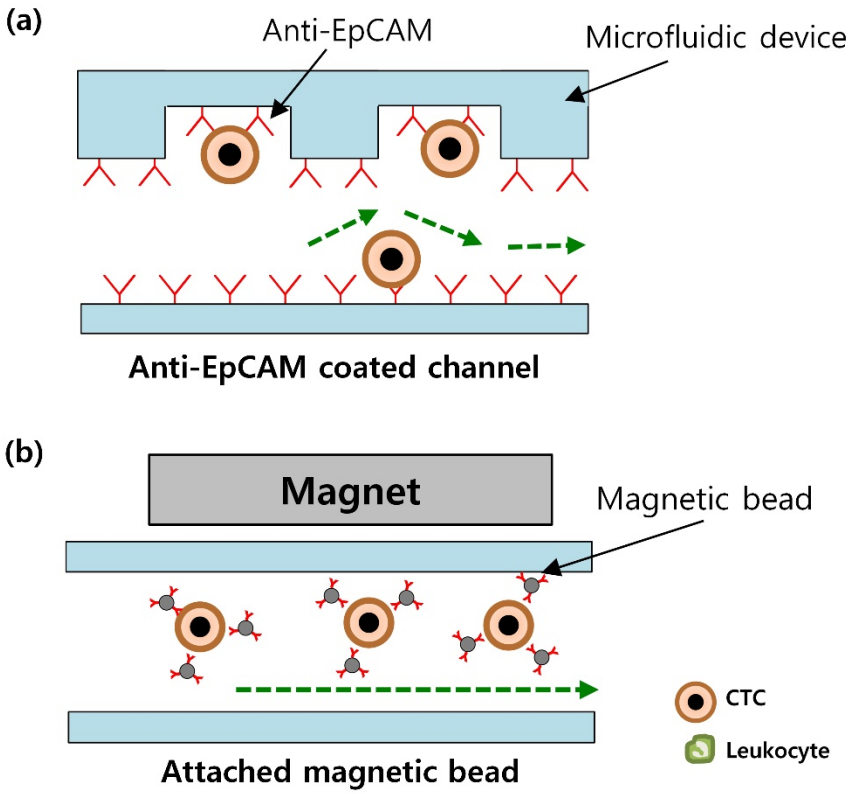

Fig 1-1. The CTCs separation method based on the antigen-antibody. (a) Ep-CAM antibodies are coated on the microchannel and the mixture sample flows. CTCs bind to anti-Ep-CAM antibodies, but the leukocyte passes through the microchannel because of the leukocyte dose not react to the Ep-CAM antibodies. (b) Before the mixture flow to the microfluidic device, antibody-functionalized magnetic beads attach only CTCs. The magnet is used to apply the magnetic field and it attracts the magnetic bead, so CTCs, which bond to the magnetic bead, are separated. On the other hands the leukocyte flows the channel regardless the applied magnetic force.

Second, CTCs have higher dielectric property than normal blood cells. The dielectric materials are the electrically insulator, but this materials can be polarized when the dielectric materials are in the electric field [53]. In an applied electric field, the electric charges freely travel through the conductive particles. In other hand, the electric charges could not flow through the insulated particles and they just shift to their equilibrium position, this phenomena is called a dielectrically polarization. During the polarization electric charges shift to equilibrium position, so the electrical charges are canceled each other and the polarized particles are electrically neutral. But the polarized particles can move under a non-uniform electric field and an alternating current (AC) field [54]. Because the irregular electric field induce the irregular dielectrophretic (DEP) force [53, 55] and this force can push or pull the electrically neutral particles in the electric field gradient. In AC field the DEP force acting on the cell is proportional to the product of the induced dipole moment and the field gradient [56]. According to the ability of polarization, DEP force easily affects to the particle or not. Claussius-Mossotti factor is used to determine how DEP force affects to the particles. Especially the real part of this factor may be expressed relation between the complex permittivities of the cell and suspending medium and it decides the direction and strength of DEP force on the targeted cell [57]. If the permittivity of the cell is higher than the permittivity of the suspending medium, the cell is attracted to regions of large spatial variation of the electric potential by the positive DEP (pDEP) force, which is called an attractive DEP, or the cell is pull from such area by the negative DEP (nDEP) force, which is called a repulsive DEP force [56]. The schematics of pDEP and nDEP are shown Fig 1-2(a) and (b), respectively. The Claussius-Mossotti factor may be expressed to the relation of the frequency of the applied electric filed and the crossover frequency, which affects to the DEP force being repulsive or attractive [58-60]. If the crossover frequency is higher than the

frequency of the applied electric field, the DEP force is repulsive and the cells are pushed from the electrode surface. The DEP force is dependent on the two types of frequency, particularly the crossover frequency is decided by the dielectric property of the cell such as the conductivity of suspending medium, cell size and cell-specific plasma membrane capacitance [53, 58, 61, 62]. Experimentally CTCs have higher value of the real part of the Claussius-Mossotti factor than blood cells, this property is used to isolate CTCs from the whole blood. The breast cancer cell lines have higher the real part of the Claussius-Mossotti factor value than the blood cells such as a neutrophils, basophils, lymphocytes and erythrocyte with frequency of applied AC field from the 10^4 kHz to 10^6 kHz. Especially at the 60 kHz, the real part of the Claussius-Mossotti factor of the breast cancer cells only is positive number and the value of the blood cells is negative number [56, 57, 63, 64]. P. R. C. Gascoyne's group used this difference of the dielectric property between the tumor cell lines and normal blood cells line to separate the breast cancer cells with high capture efficiency, which is up to 92% [57]. The nDEP based electrosmear method [65] was introduced to separate and settle the various kinds of cells on the electrode using the negative DEP force or a sedimentation force. In this study the crossover frequency was fixed, so the DEP force dependent to the frequency of the applied electric field. The different frequency field was applied on the different site of the electrode array and the different DEP forces acted to the flowing cells. The cell flew a zone and the cell was pushed from the electrode by the repulsive DEP force, because of the crossover frequency was higher than the frequency field of this zone. But when this cell passed to the other zone, the attractive DEP force pulled the cell to the electrode because of the crossover frequency was higher than the frequency field of this area. Result in the MDA-435 (breast cancer cell) cells, granulocytes and erythrocytes were settled on the different zones applied 57-74 kHz, 192-231 kHz and 298-345 kHz,

respectively [65]. The DEP separation, the isolated CTCs are viable to subsequent analysis and it is possible to culture in laboratory environment [53, 57]. This method can isolate CTCs selectively due to the specificity of the dielectric phenotype of cells [66]. Despite of several advantages like a non-labelling method and high viability of the isolated cell, the DEP based separation method needs an external energy source to apply the electric field to the microfluidic device. Because CTCs must remain spaced to avoid dipole–dipole interactions that can perturb the DEP responses [53, 57], this technology requires the enough spacing and it offers low throughput. Also the blood is a high conductive medium, this medium can affects to the permittivity of the CTCs and this property of the blood disturbs the separation process.

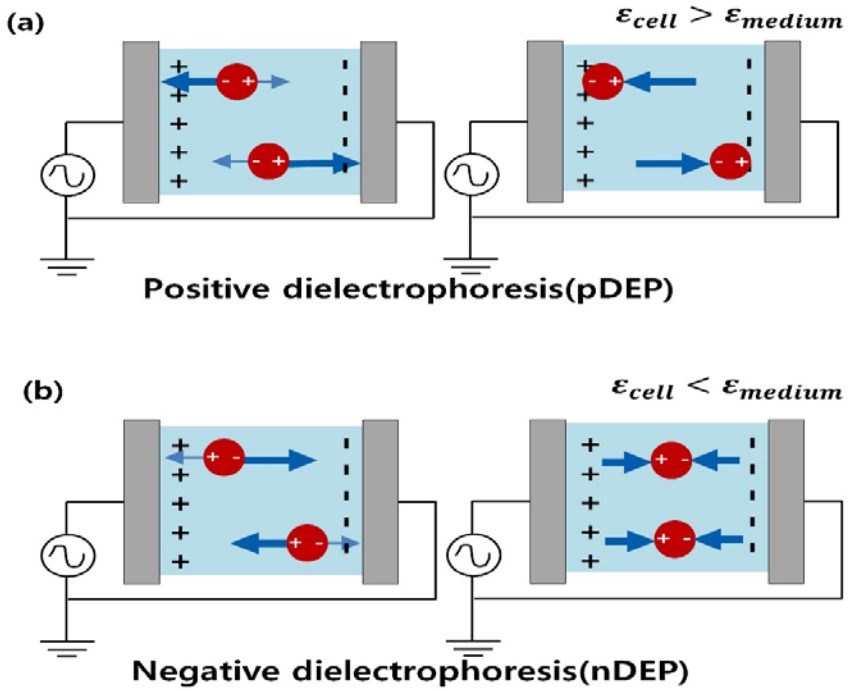

Fig 1-2. Schematics of the pDEP and nDEP are (a) and (b), respectively. In the applied AC electric field, the electrically neutral cells (red cells) are polarized and experience the electrical forces. If the difference of the permittivity of cell and medium, the polarized cells are pushed or attracted to the electrode.

Third, CTCs are stiffer and less deformable than other blood cells. Elasticity of cells is one of the distinguish property and this property is used to a physical cell marker. The elastic assets of cells can increase or decrease depending on the biologic changes during the progressive stage of pathogenic processes [67, 68]. The cytoskeleton governs an internal structure of most cells, which is constituted of the biopolymeric molecules [69]. The cytoskeleton can determine the mechanical strength and morphology of the cell and this protein is involved to the elastic changes of the cells during the differentiation processes of the normal cells as well as the developmental stages of pathologic various diseases [70, 71]. Decreasing of the cell stiffness means an increasing of the mobility and invasiveness character of the cell, the measurement of the elasticity of targeted cell can work like a biopsies. The deformability property of the cell is considered to the indicators of the various diseases including cancer and blood disease, including the cancer [67, 69, 71, 72] or blood diseases [73-75]. In cases of the circulating normal cells or CTCs, they are more deformable than the other cells, which is not circulate, because they can escape from the original tissues and circulate to the blood or lymphatic stream, and in particular CTCs invade to other organ for spreading out [76]. The young's modulus is related to the stiffness of the elastic materials, the measurement of this modulus of the cells can help to determine the changes of the cytoskeleton and the stiffness of the cells [77]. By the scanning force microscopy (SFM), which is using the liquid cell and laser deflection technique, the Young's modulus of the normal cell lines from a non-malignant ureter (Hu609), a non-malignant bladder urothelium (HCV29) and the cancerous cell lines such as HCV29 cells transfected with v-ras oncogene (BC3726), bladder transitional cell carcinoma (T24) and bladder transitional cell carcinoma (Hu456) [77]. The interaction between the probing tip and the cell surface makes a laser deflection, the photodiode collects the light, and the computer gets the data from the

photodiode and analyses the laser alternation. After Young's modulus of reference is measured using the glass, the Young's modulus of the liquid cells are measured. The Young's modulus of the normal cell lines are higher about 10 times than this modulus of the cancerous cell lines as figure 1-3(a). S. E. Cross and colleagues [78] measure the stiffness of live metastatic cancer cells extracted from pleural fluids of lung cancer patient, breast cancer patient and pancreatic cancer patient using atomic force microscopy (AFM). They found that these metastatic cancer cells were deformable 70% more than the benign cells in the sample fluids. Young's modulus of the metastatic cancer cells was 0.53±0.10 kPa and the benign cells was 1.97±0.07 kPa [51, 78]. In summary, the cancer cell is almost 10 times stiffer than the blood cells (leukocytes) and the metastatic cancer cell is more deformable about 3 times than the non-metastatic cancer cells. The elastic character of the blood cells and cancer cells certainly different, it can be used to isolate the CTCs. In this reasons, the comparison of the elastic properties between the blood cells (especially leukocytes) and CTCs is important for the physical separation of CTCs from the blood sample [51]. Using the elastic property to isolate the CTCs, there are several separation microfluidic devices like a filtration chip [79-81], moreover a mechanical separation chip (MS-chip) [82] were developed to separate between the metastatic cancerous cell and non-metastatic cancerous cell, which cells have different elastic property. Figure 1-3(b) shows the example of the deformability based micro pillar array. The filtration chip was designed to a long serpentine channel with the aperture array to separate the blood cells and CTCs [79]. Basically other cell filer or cell sorter devices use the fluid pressure to sort the targeted cells by passing or clogging the traps. The filtration chip was differently design with the filter array to taller height and smaller width than size of CTCs for preventing the cell lysing. If CTCs are clogged or filtered in the smaller height and width trap gap, CTCs cover the trap opening completely and the tension of cell

membrane increased. This result in the probability that the trapped cells get the damages to lysing and the cell viability decreases. Also the taller height of the aperture may trap multiple CTCs simultaneously. Two aperture arrays are consisted in main straight channel and the bending aperture array are lied in the bending out channel, which the sample flow direction are changed. The bending aperture array is not exactly located on the outer of bending channel, this array is placed an end of the bend U-shape channel to prevent the leaking of CTCs by the change of the fluid momentum. The trap array is finally located after the long serpentine micro-channel to separate the remained CTCs from the sample flow. CTCs spiked blood sample flows this serpentine channel and the separation between the blood cells and CTCs are based on the fluid pressure. The blood cells are small and more deformable than cancer cells, so they can pass through the trap array, but the large and less deformable CTCs are filtered and clogged at the trap array. The removed blood cells flow the both sides of different channel from the main channel and they are collected to waste outlet. After the blood cells are removed from the sample, the recovery was high as 90% at 25uL/min flow rate. The CTCs are larger and stiffer than the blood cells, they could not travel through the aperture. Weijia Zhang, et al. [82] designed the MS-chip to study the difference the deformability property between the metastatic CTCs and non-metastatic CTCs. The micro-barriers are embedded in MS-chip and this chip uses the hydrodynamic force to isolate the deformable cells from the stiff cells. The gap between the micro-barriers become small from 15㎛ to 7㎛ according to the downstream, the stiffer cells are trapped and softer cells pass through the micro-barrier. They tested the two different breast cancer cells MCF-7 and MDA-MB-436 (metastatic breast cancer cell). Because the stiffer cytoskeleton and the metastatic property is related to the deformability, non-metastatic cancer cell MCF-7 is stiffer than MDA-MB-436. From the inlet to outlet the less deformable cells were trapped regardless to

the cell type. MCF-7 cells generally retrained in the microfluidic device, the proportion of MCF-7 was near the 30% and the proportion of MDA-MB-436 was 80% after the separation. The result shown the cell size is not important factor during the experiment, the small stiffer cells are clogged and large softer cells travel the MS-chip. When the apertures or filtration geometry are smaller than the cells, the cells cover the gap between the trap and other trap post. The fluid continually flow forward to the trap array, the fluid pressure increases by the blocked pass load. The increased fluid pressure makes the cells experience the force and get the damage to the cell lysis. The cell damage offers the probability to cell lysis and loss of the cell [79, 81]. Another limitation of filtration method is clogging. The clogging of CTCs changes the fluid flowing, it saturates and decreases the capture efficiency [80]. The reverse flow was applied to overcome this limitations, the results were no clogging and no decreased capture efficiency during the operating time that was more than 4 hours [79, 83]. Long separating time means the low throughput.

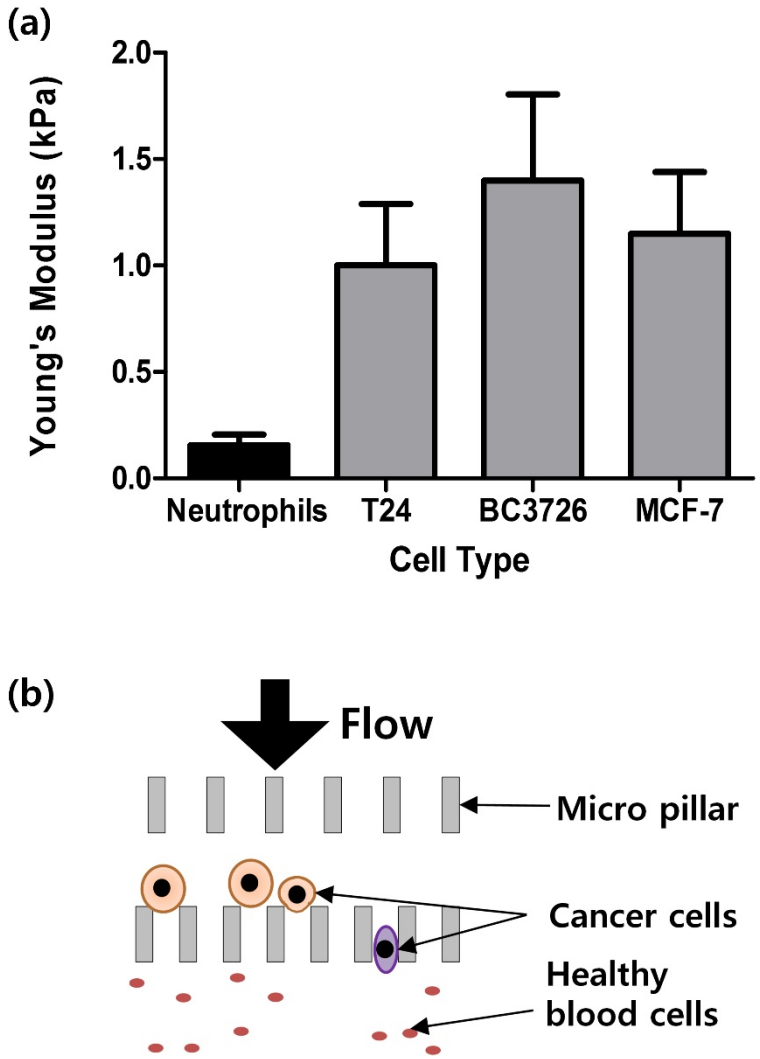

Fig 1-3. (a) The graph shows the Young's modulus of several cell type. Young's modulus of the neutrophils, the cancer cells like T24, BC3726 and MCF-7 cells. The values of Young's modulus of the cancer cells are higher approximately ~10 times than the neutrophils, the cancerous cells are stiffer than neutrophils [51, 77, 78]. (b) Microfluidic device can separate the cancer cells from the blood cells based on the stiffness difference. The large and stiff cancer cells are clogged or take long time to pass the pillar array and small and deformable blood cells pass through the micro-barriers.

Fourth, CTCs are larger than the blood cells. As shown figure 1-4(a)., the number of CTCs in the 1ml of blood is very rare to $1\sim10^4$ cells/ml with comparison with the number of the leukocyte $\sim10^7$cells/ml and the erythrocyte $\sim10^9$ cells/ml [32, 33, 84]. The size of CTCs are larger than red blood cells and white blood cells [85]. CTCs size ranges from 12 ㎛ to 25 ㎛ [86], the leukocyte size ranges from 7 ㎛ to 15 ㎛ and the erythrocyte size ranges from 7 ㎛ to 10 ㎛ [87, 88]. A neutrophil occupies the most of portion of leukocyte, the population of the neutrophil is 62% and the size of neutrophil is from 12 ㎛ to 15 ㎛. Moreover almost of the leukocytes are smaller than 15 ㎛. The size is overlapped between the leukocytes (such as the neutrophil) and CTCs, its rage is 12 ㎛ to 15 ㎛. Despite of the overlapping of size rage, the sized based separation can efficient because of CTCs is large up to 25 ㎛. Using this difference of the cell size, the separation technology are developed. Because the cell diameter is different between CTCs and the blood cells, the different sized-cells experience different magnitude of forces. Photophoresis [89] is the phenomenon that the particle included to the fluid can move by induced force in the volume of particle, it is illustrated at figure 1-4(b). The applied light scatters to near to the fluid and the particle, which suspended in the fluid, absorbs the energy. The energy can be turned to an irregular heat distribution in the volume of particle, consequently the irregular heat distribution can create a force to make the particle to move [89-91]. If the high absorptive particle absorbs more energy than surrounding fluid on the surface of the particle, the particle moves away from the optic source. But if the low absorptive particle absorbs less energy than fluid on the rare surface of the particle and the fluid absorbs more energy than the particle, becomes hotter than the front surface of the particle and the particle moves forward to the light source [89, 91, 92]. By the equilibrium of the drag force induced by fluid flow and the

photophorestic force induced by given wavelength. The former case is positive photophoresis and the latter case is negative photophoresis. Hongxiang Lei' groups [92] researched the relationship between the photophorestic force and the multi-size particles. They used the negative photophoresis induced by the leaking wavelength from the optical fiber in the microfluidic device. Especially the optical fiber was placed in the U-groove shaped channel, which located to the middle of main microchannel vertical to the fluid flow direction. The wavelength of the optical fiber was 1.55 ㎛. The particles with a very low absorption coefficient flow the microchannel by the applied fluid flow and the optical fiber leaked the light at the middle of the device. The particles in the fluid experience the drag force and photophorestic force, consequently the particles are focused to different distance. According to the particle's size the retention distances were different. The large particle has a large asymmetry factor of energy distribution within particle [93], which is an inverse proportion to the retention distance. Therefore the large particle stay at the large distant from the optical fiber and the multi sized particles are separated. Another method for sized based separation, the passive separation methods induce changes in particle behavior using hydrodynamic effects that are driven by the geometrical features of microchannels [94]. Jae-Sung Park's group [94, 95] designed the multi-orifice microfluidic system to separate the multi sized particle. The multi-orifice geometry is the contraction and expansion shape. The width of the contraction area is 40 ㎛ and those of the expansion is 200 ㎛. The fluid flows the expansion chamber, the vortex shaped flows are generated and the fluid in the main channel flows straight. When the small particle enter from the contraction chamber to the expansion chamber, this particle flows along the streamline. However the large particle travels rapidly from the contraction area to the expansion area, the particle experiences mismatching

between the fluid streamline and inertial direction of the particle. The mismatching is occurred by inertial force induced the momentum change of the particle. From the upstream to downstream, the particles are focused. In the result, the small particles are divided two way near the wall side and the large particles are focused on the centerline after the several multi-orifice segment. Moreover they tested MCF-7 cells spiked blood sample with multi-orifice microfluidic system. Using this microfluidic system, CTCs were separated with the capture efficiency of 88.8% and the purity of 1.5%. The size based isolation technology can offer the several advantages such as non-labelling for the cell viability, the high throughput and less cell damage [33]. Especially the hydrodynamic separation method can separate CTCs without the external source, and because CTCs are isolated using the passive geometry without the effect of the fluid pressure and clogging, the hydrodynamic separation method can offer the high throughput and less cell damage [94, 95]. But the common limitations of the photophoresis based and the hydrodynamic based separation are that the size of CTCs are overlapped to the size of the leukocytes and the conditions of the suspending fluid significantly affects to the separation results [83, 96, 97].

(a)

Cell type	CTC	Erythrocyte	Leukocyte
Cells/㎖	1-10^4	~10^9	~10^7
Size(㎛)	12-25	5-7	7-15

Cell type	Neutrophil	Lymphocyte	Monocyte	Eosinophil	Basophil
Size(㎛)	12-15	7-15	12-15	10-12	12-15
% of Pop	62	30	5.3	2.3	0.4

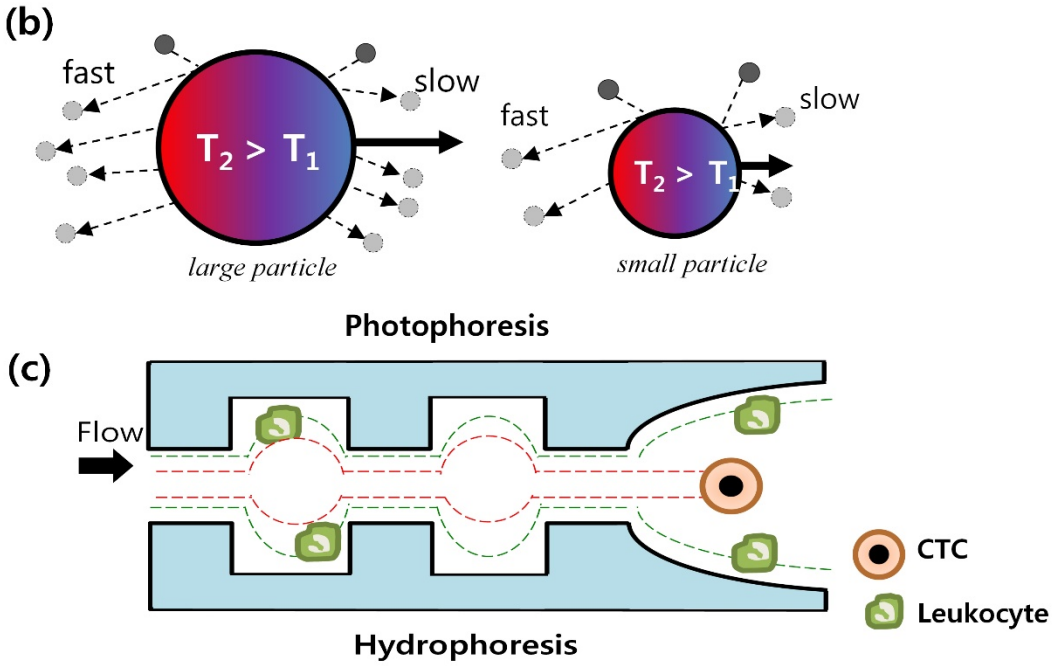

Fig 1-4. (a) The graph shows the difference between the blood cells (red blood cells and white blood cells) and CTCs [32, 33, 84-88]. CTCs are generally larger than other blood cells, and extremely rare in the blood. % of Pop means the percentage of the population. (b) Photophoresis of large particle and small particle. The large particle experiences stronger photo-induced force than small particle. (c) Hydrodynamic separation technology is shown. CTCs and leukocyte flow to different focusing position.

In summary, the microfluidic based technology for separation of CTCs grounded the physical properties like the Ep-CAM on the cancer cell surface with Ep-CAM antibody or antibody-conjugated magnetic particle, the higher dielectric property, the less deformability and the larger size than the other blood cells as table1. Several parameters are used to evaluate the separation technology such as the capture efficiency and the capture purity, throughput or the cell viability. Among these parameter, the key parameters to evaluate these separation technologies are that how the targeted cells are collected without missing, how much the wasted or non-targeted cells are removed from the collected sample and how much the sample are processed [98], shown as equation (1.1) and (1.2). Because the molecular analysis for the medical decision or the cancer research is very important to the patient and doctor, and the researcher, these parameters are the important parameters. Using these parameters, the separation technologies are evaluated.

$$\textbf{Capture efficiency} = \frac{Target\ cells_{outlet}}{Target\ cells_{inlet}} \tag{1.1}$$

$$\textbf{Capture purity} = \left(\frac{Target\ cells}{Total\ cells}\right)_{outlet} \tag{1.2}$$

Ep-CAM antibody only binds to specific antigen, CTCs are sensitively and selectively isolated despite of the diverse types of CTCs. Moreover the Ep-CAM functioned magnetic particle attaches and drives the targeted cells by the magnetic forces in the applied magnetic gradient. But the one of the key disadvantage of this method is the immunological method is the labelling method. Nonetheless the labelling method is sensitive, the labelling decreases the viability of cells and it is challenge to identify and analyses the isolated cells. Another of difficulty is that the diverse types of antibodies are needed to detect to the various heterogeneity of CTCs and detaching problem after the binding and separating process. In the

negative enrichment technology case, CTCs are isolated without the antibody binding and the antibody is required to detect the blood cells. But the number of blood cells is large and the required antibody of blood cells, the large enough area and antibody are needed to bind the very large number of blood cells. The dielectrophoresis technology uses the difference of dielectric property. The higher dielectric property of CTCs is non-labelling and it can offer the high cell viability with compare to the immunological method. To use this method, the additional equipment are used to apply the electric field. Also the blood is high conductive medium and the gap dielectric property between the blood cells and CTCs is not dominant in the blood, the sensitivity is lower than immunological method and the throughout decreases. Other method uses different deformability that CTCs are stiffer than blood cells, CTCs are isolated without the labelling and external forces. Inertial force affects to cells. When the cells faces the filter geometry or trap arrays, the softer cells deform their structure and pass the filter or trap but, the stiffer cells are clogged and stuck. It has limitations that clogging occurs the cell damage and decreased cell viability, and the trapped CTCs should be extracted after filtration. The different size of CTCs and blood cells is useful to separate CTCs without labelling other external forces. Using the specific geometry not the filtration and inertial force of fluid, this method decreases cell damage and increases the cell viability. One of the problems of this technology is the overlap of size between the blood cells (leukocytes) and CTCs, the specificity is low. The two kinds of cells are similar in 12㎛ to 15㎛, the same size but different type of cells are separated same outlet. To efficiently separate CTCs from the blood and analyses them, several key required factors such as the non-labelling and non-external forces, high cell viability and throughput. Also the high capture efficiency and the capture purity are essentially required to subsequent molecular analysis for the diagnosis, treatment, development of the new drug or biomarker. The overlap of size is limitation of the

size based hydrodynamic separation, it can meet the required factors with the non-labelling and external forces, high cell viability and throughput.

Property	Method	Principle	Advantage	Disadvantage
Antibody-antigen reaction	***Immunological***	-Specific antibody-antigen reaction	-Sensitivity -Specificity	-Particular antibody -Detaching antibody -Require large area
	Magnetic	-Magnetic labeling to target cells -Isolation by magnetic force	-High affinity -Recovery by removal of magnetic field	-Low throughout -Exogenous labeling -Require large area
Dielectric-property	***Dielectric***	-Dielectric properties of targets in electric field	-Non-labeling -High cell viability	-Using external force -Low throughput -High conductivity medium
Stiffness	***Filtration***	-Inertial force and deformability of cells	-Non-labeling -High throughput	-Clogging and Cell damage -Extraction targets
Size	***Optical***	-Using a photophoretic force	-Non-labeling -High throughput -Less cell damage	-Using external force -Extraction targets -Overlap of size
	Hydrodynamic	-Inertial force of cells in the fluid	-Non-labeling -High throughput -Less cell damage	-Overlap of size -Effect of flow condition

Table1. Microfluidic technology for the separation of CTCs from the blood.

1.3 Current research and principle

The hydrodynamic separation gets the attention and it is considered to the proper separation method. Nonetheless the limitations of the same size range between CTCs and leukocytes to disturb the complete isolation, this technology can satisfice the several required factors such as the capture efficiency, capture purity, thigh cell viability or less cell damage, and the high throughput. Therefore, the hydrodynamic separation technology is continually developed. When the particle is included in the fluid, the movement of the fluid and particle in the microfluidic system is analyzed by the forces acting to the fluid and particle and dimensionless numbers. Reynolds number (*Re*) is composed by the ratio between the inertial and viscous effects of the fluid, this dimensionless number is used to interpret the behavior of the fluid. The high or low *Re* means that the inertial force affects dominantly to the behavior of the fluid as a turbulence or the viscous force affects dominantly to the behavior of the fluid as laminar flow [99]. In the microfluidics, the channel Reynolds number (Re_c) are used to describe the fluid behavior with changing the mean fluid velocity to the maximum fluid velocity. If the particle is suspended in the fluid and this particle travels with the flowing fluid, the behavior of the particle is interacted with the inertial force and viscous force of the fluid and the particle's movement is affected by the particle size and the diameter of a channel. The particle movement is interpreted by using the particle Reynolds number (Re_p) [100]. The *Re*, Re_p and Re_c are expressed as

$$Re = \frac{U_{mean} D}{\mu} \tag{1.3}$$

$$Re_c = \frac{U_m D}{\mu} \tag{1.4}$$

$$Re_p = Re_c \frac{a^2}{D_h^2} \tag{1.5}$$

where U_{mean} is the mean fluid velocity, D is a diameter of channel, μ is the fluid viscosity, U_m is the maximum fluid velocity, a is the diameter of particle and D_h is hydraulic diameter of channel. The condition at $Re_p \gg 1$, the inertial force is dominant parameter to make the particle to migrate laterally. Opposite condition at Re_p<<1, the particle strongly experiences the viscous drag forces and the particle flows along the fluid flowing. Other number for describing the behavior of the particle is the Stokes number (St). When the particle faces the accelerating fluid, the behavior of the particle can be established. This dimensionless number is composed the ratio the relaxation time (τ_p) of the particle to the characteristic time (τ_f). It follows as,

$$\mathrm{St} = \frac{\tau_p}{\tau_f} = \frac{\rho_p a^2 / 18\mu}{D_h / U_m} = \frac{\rho_p a^2 U_m}{18\mu D_h} = Re_p \frac{\rho_p}{18} \tag{1.6}$$

where, ρ_p is the density of particle. Stokes number is related to the particle Reynolds number and the density of particle. If the condition of St << 1, the particle flows along the fluid flow. At the opposite condition of St >> 1, the particle keeps its original trajectory regardless of the streamline. Using this dimensionless number decides the behavior of the particle. Therefore the particle with large St and Re_p equation (1.5) flows the microchannel with mismatching from the fluid flowing. When the particle enters to the straight microfluidic device, the drag force makes to the particle to flow and the two kinds of forces affect to the particle to lateral migration; shear gradient induced lift force and wall effect induced force [99, 101]. Figure 2-1(a) shows the particle behavior in the micro scale channel. In the microchannel, the flow profile is parabolic and the centerline of fluid flows with the

maximum velocity and the velocity of the wall side is 0. As the velocity of the wall side is 0, the fluid profiles shapes the parabolic and the fluid on the center line flows with the maximum velocity. The maximum fluid velocity is same to the 2 times of the mean fluid velocity. The particle in the straight microfluidic system, it flows with Poiseuille velocity profile. By the fluid velocity gradient, the particle experiences the shear induced lift force [102]. The relative fluid velocity on the surface of particle at the wall side is higher than those of particle at the center side. Basic to the Bernoulli's principle the increasing fluid velocity simultaneously occurs the decreasing of pressure, the relative fluid velocity on surface of particle at the wall side is high and the pressure of that site decreases. Therefore, particle is pushed to the wall side by shear gradient induced lift force. When the particle migrates near the wall side, the particle experiences the wall effect induced lift force [103]. By the approach of the particle to the wall side, the wall side fluid velocity surrounding of the particle becomes slow and the pressure increases. Also the particle blocks the fluid flowing near the wall side, the weaken vortex are generated. The generated weaken vortex pushes the particle from the wall side to the center line as figure 2-1(b) and (c). Therefore the acting direction of the shear gradient induced lift force and the wall effect induced lift force opposite each other, and the equilibrium of two forces determine the equilibrium position of particle in the microchannel [99, 102-106]. This phenomenon is known the tubular pinch effect, which was experimentally observed by Segre and Silberberg in 1962 [101, 107]. When the particles entered to the channel, uniformly dispersed particles migrated to form a narrow band near the channel walls. This narrow band is equilibrium position of the particle. The lateral migration of particle in the fluid pipe is proportional to the radius of pipe and the focusing position is estimated to about 0.6 radius from the axis of pipe.

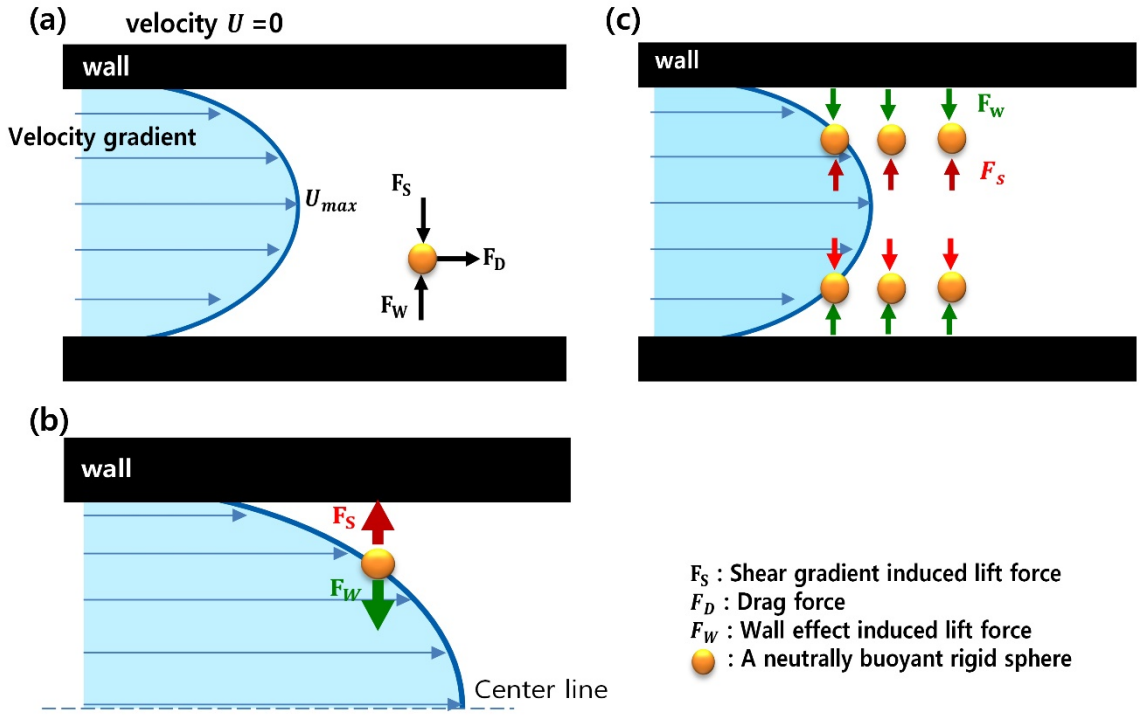

Fig 2-1. The illustration of the tubular pinch effect is shown. (a) The fluid enters to the microchannel, the profile of fluid is parabolic shape and the fluid velocity is maximum almost two times of average fluid velocity at center of fluid profile. The fluid velocity at the wall side is 0. When the particle in the microchannel, the particle experiences three types of forces. Drag force, shear gradient induced lift force and wall effect induced lift force affects to the particle. (b) F_S and F_W affect to the particle, F_S derives the particle from center line to wall side and F_W pushes the particle from the wall side to center line. (c) By the equilibrium between two forces, which are F_S and F_W, the particle flows at the focusing position in the microchannel.

Multi-orifice flow fractionation (MOFF) [94, 95] is the size based hydrodynamic separation method. The geometry of MOFF was designed the contraction and expansion chambers, which called multi orifice. In the straight microchannels that is long enough to isolate the particles only based on the tubular pinch effect, the particles can flow along the their focused position with difference of the particle size. If the straight microchannel suddenly expands, the dimension of the walls significantly increases and the fluid stream generates the vortex flow or separated flow. By expanding the channel dimension, the Reynolds number increases and the large scale secondary flow are formed at the wide channel. At the first straight channel, the randomly flowing particles flow and the tubular-pinched particles are concentrated their equilibrium position. The compared with the behavior of particles in the contraction channel by the balanced two lift forces, the particles experience very weaken wall effect induced lift force because of the increased distance between the wall and the centerline in the expansion channel. The shear gradient induced lift force dominantly affects to the particles, the particles are derived to the wall sides. The most of the particles are effect of the fluid flowing line and they are focused near the sidewalls by through a series of the contraction/expansion chamber. But the particles pass a number of MOFF geometry and the particles gradually migrate to two way. For the size based separation the momentum change induced lift force affects to the particle trajectories [94, 95, 108, 109]. The momentum change induced lift force is based on a mismatching between the fluid flowing line and the particle trajectories. In the expansion geometry the particles experience the sudden change of the momentum with high Re_p and St, the mismatch of direction between the fluid and particle flowing occurs. The inertial force affects the particles to escape the deriving fluid streamline and to stick to the original trajectories of the particles. The particle trajectories are accumulated and amplified while the particles travel the MOFF

device. The focusing positions of particles are decided with the balance of the inertial force, which is related to the momentum change to lateral migration of the particles, and the drag force, which derives the particles movements. The momentum change in a certain time interval (Δt) is driven from the Newton's the second law and the inertial force of the particle is equal. The equation related to the momentum change $\Delta(mv)$ and the inertial force (F_i) can be estimated as

$$F_i = ma = m\frac{dv}{dt} \sim m\frac{\Delta v}{\Delta t} = \frac{\Delta(mv)}{\Delta t} \tag{1.7}$$

Time interval is corresponded to the characteristic channel dimension (D_c) over the average fluid velocity (U_a). The inertial force is transformed as

$$F_i \sim m\frac{U_a^2}{D_c} \quad , \qquad \left[t = \frac{distance}{velocity}\right] \tag{1.8}$$

The volume of sphere equation related to the radius of the sphere is substituted and then the inertial force can be expressed as

$$F_i \sim \frac{\rho_p \pi a^3 U_a^2}{6D_c} \quad , \qquad \left[volume\ of\ sphere = \frac{4}{3}\pi r^3\right] \tag{1.9}$$

The lateral migration will be balanced by Stokes drag force (F_d), which derives the particle to move in the fluid environment, and the particle migration velocity U_d is calculated by

$$F_i = F_d = 3\mu\pi a U_d \tag{1.10}$$

$$U_d = \frac{\rho_p a^2 U_a^2}{18\mu D_c} \tag{1.11}$$

The particle migration velocity is proportional to the square of the particle diameter and the square of the mean velocity of the fluid while the other parameters are constant

regardless of a^2 and U_a^2. When the fluid velocity is same, the particle size is the key parameter to separation. Also, U_a is similar to the St with multiplied the fluid velocity. This means the trajectory of large particle easily mismatches to the fluid direction than those of the small particle. Therefore the large particles migrated to the center of channel and the small particles focused two side near the walls. The multi sized particles are randomly injected, focused to their equilibrium position and separated based on the particle size, the principle of MOFF is shown at figure 2-2(a). Using the MOFF system, MCF-7 cells were separated from the cancerous cells spiked blood sample with diluted 1:100 buffer. With diverse channel Reynolds number from the 30 to 90, the blood cells and cancerous cells were tested. At the 70 of channel Reynolds number, RBCs, WBCs and MCF-7 cells were separated respectively. In results the capture efficiency was 88.8% and the capture purity was 1.5% [94, 95, 110]. The more investigation is needed to overcome the effect of volume fraction and the variable flow rate should maintain.

To improve the low capture efficiency and poor purity of single stage MOFF, the multi-stage MOFF (MS-MOFF) [111, 112] was designed as figure2-2(b). MS-MOFF was composed the first and second stage multi-orifice segment, the end of the first stage was divided to three channels. The divided two side channels were connected to the second stage for re-separation and the middle channels was linked to the cancer cell collected outlet. After the first stage, the cancer cells was isolated to the middle channel and the blood cells flown to the second stage. In the second stage, re-separated cancer cells were collected to cancer cell collected outlet and other blood cells are removed to the waste outlets. The $1x10^4$ cells/ml cultured MCF-7 cells in blood sample was diluted with buffer 1:100. The capture efficiency was 98.9% and the capture purity was 0.3%[112]. The capture efficiency was almost 100%, which was higher than single stage MOFF, but the capture purity was almost

0% and it was lower than single stage MOFF. Another series of MOFF is the parallel MOFF (p-MOFF) was developed to increase the throughput and test the blood sample derived from the metastatic and adjuvant patients [113]. This chip was comprised to the filtration area and the parallel four single stage MOFF like figure2-2(c). From the filtration area the channel was divided to four-single stage MOFF and the waste outlets each other and cancer cells outlet each other were linked to collect the blood cells and cancer cells, respectively. The diluted 1:10 with buffer blood sample with MCF-7 cells and MDA-MB-231cells was injected to inlet, the cells passed through the filter zone and then traveled the single stage MOFFs. In result the capture efficiency of MCF-7cells and MDA-MB-231 cells were 93.75% and 91.60%, respectively[113]. The common limitations of MOFF series is the dilution process of blood sample and the low capture purity. Because the number of the blood cells is extremely larger in the blood sample than those of CTCs, the dilution process is used to decrease the number of the blood cells and to make the isolation to easier than intact whole blood sample. However, the number of CTCs in the derived whole blood sample from the cancer patient is really rare than the experimentation, the dilution process decreases the number of CTCs and the capture purity. These limitations should be solved to apply this separation technology with whole blood sample without the dilution for POC (point of care).

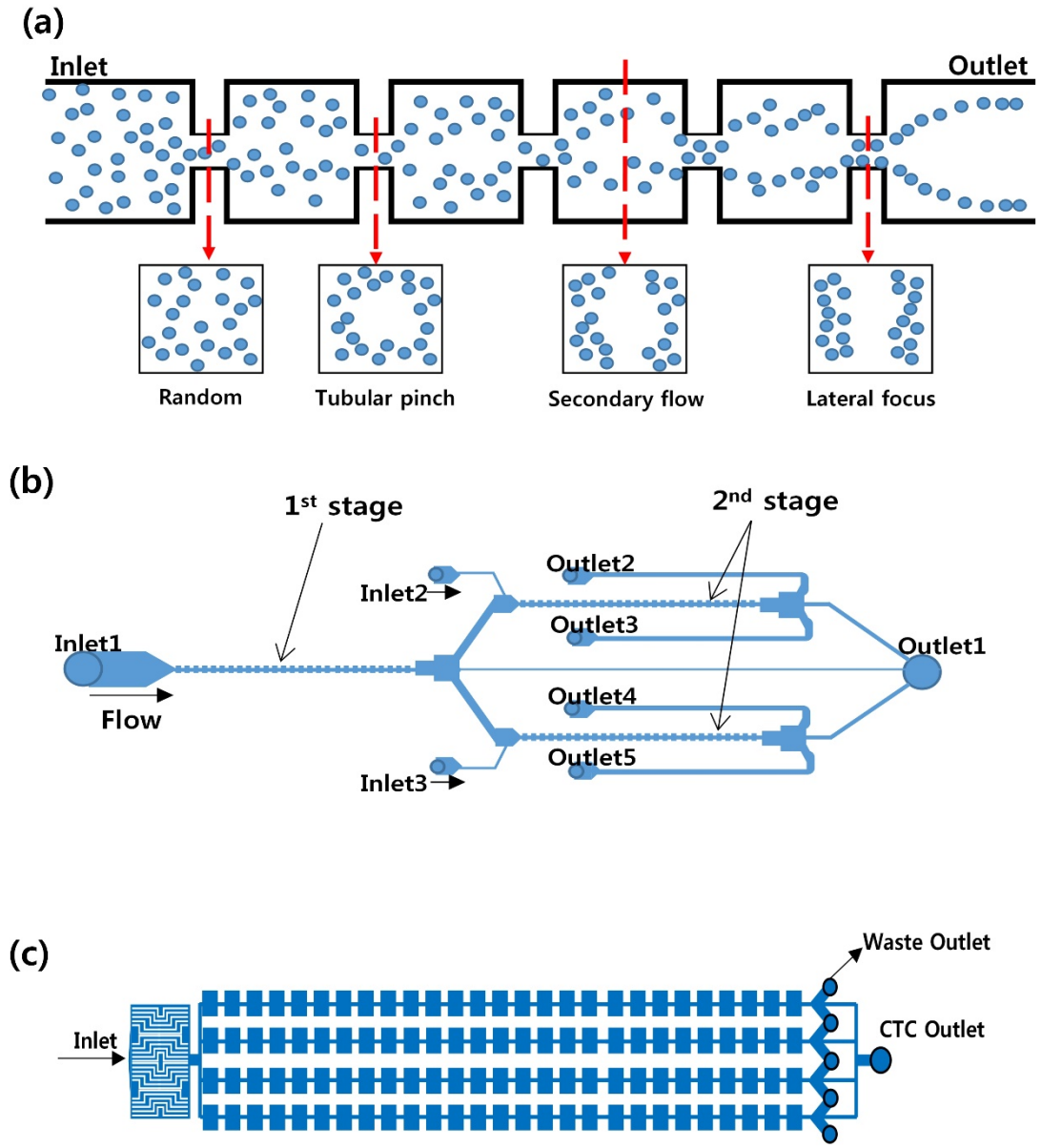

Fig 2-2. The figure is the MOFF series. (a) The principle of MOFF and the particle behavior in the MOFF system are illustrated. From upstream to downstream, the randomly injected particles in MOFF are laterally separated and focused. (b) Multi-stage MOFF (MS-MOFF) is composed to fist stage multi-orifice segment and second stage multi-orifice segment. This microfluidic has one sample inlet, two buffer inlets for re-separation in the second stage, outlet1 is for MCF-7 and four outlets (outlet2, 3, 4, and 5) are for blood cells. (c) Parallel MOFF (P-MOFF) is design the filter area and four multi-orifice segments. CTCs go to the center outlet and the split blood cells go to the waste outlets.

A DLD (deterministic lateral displacement) [114] was suggested to separate the targeted cells from the complex mixture, using the property of the larger or smaller size of the targeted cells than non-targeted cells. DLD was composed with the micro scale post array, which was laterally shift array to compare to the previous row from the upstream to the downstream. The deterministic posts were periodically arranged with a shift fraction (λ), a center-to-center length (D) and the gap length between the posts (g) and an every subsequent micro scale post array is shifted as λ D with regular g [115, 116]. When the fluid flows through the DLD device, the number of the divided stream lanes are same to the inverse of the shift fraction value and the divided stream lanes differently flow through the deterministic post array, respectively. Flowing stream lanes originally located to a position as the initial position in order 1/ λ row. The total flux of fluid stream is regular at each gap, the divided with ε of the fluid flux at the gap is same to the flux of the each stream lane. If any stream lane, the other stream lane. The width of the center stream lane is narrow and the width of the side stream lane become wider. Because the fluid velocity at the obstacles is zero, the shape of the fluid is a parabolic profile and the fluid velocity at the center of fluid stream is higher than those of other stream lane. So, the width of the stream lane is not necessary to same and the width of each stream lane can change according to the fluid velocity [115].

$$\int_0^{\beta} u(x)dx = \lambda \int_0^{g} u(x)dx \qquad (1.12)$$

Where β is the width of a first stream lane, the flux of fluid at the first stream lane is equal to the ε times of the total flux of fluid flowing the gap. For example as figure 2-3(a)., if the post array are shifted with the shift fraction 1/3, the number of stream lanes (orange, yellow, blue) was 3. The divided stream lane flows the microchannel and the position of the stream lane is original at the third row. At the inside of the gap the width of stream lane is

different, the wall side stream lane is wider than the middle side stream lane since the fluid velocity is slower than the middle site. If the radius of the particle is smaller than the width of the first stream lane, this particle flows along the fluid flowing. This particle flows with the first stream lane and its position is same to the original position at the third row as figure 2-3(a). In opposite case, if the radius of the particle is larger than the width of the first stream lane, this particle travels away from the initial position to outer position and it flows same stream lane as shown figure 2-3(b). The smaller particle flows in 'zigzag mode' and the larger particle flows in 'bumping mode'[115]. The parameter for division between the zigzag mode and the bumping mode is the critical radius, R_c, which is equal to the width of the first stream lane. R_c is determined the path of the particle in the DLD system, it is expressed as

$$R_c = \beta \tag{1.13}$$

R_c can be described with the gap, the row shift fraction and the variable parameter, η, to adapt for irregular fluid profile through the gap.

$$R_c = \lambda g \eta \tag{1.14}$$

The assumption of the flow profile is parabolic shape, the width of the first stream lane is analytically founded as function of λ, it is solved to find the cube root with involving to the equation (1.12).

$$\left[\frac{\beta}{g}\right]^3 - \frac{3}{2}\left[\frac{\beta}{g}\right]^2 + \lambda\frac{1}{2} = 0 \tag{1.15}$$

Using equation (1.13), the equation (1.15) can be rewritten the cubic equation, g works as the consistent and the w is the root related to the λ, expressed as

$$R_c = g\left[1 + 2w + \frac{1}{2w}\right] \tag{1.16}$$

$$w^3 = \frac{1}{8} - \frac{\lambda}{4} \pm \sqrt{\frac{\lambda}{16}(\lambda - 1)}\,. \tag{1.17}$$

The correct root of w^3 is

$$w = \left[\frac{1}{8} - \frac{\lambda}{4} \pm \sqrt{\frac{\lambda}{16}(\lambda - 1)}\right]^{1/3} \left(-\frac{1}{2} - i\frac{\sqrt{3}}{2}\right). \tag{1.18}$$

Hence, the ratio between λg and η determines the critical radius of particle.

$$\eta = \frac{R_c}{g\lambda} \tag{1.19}$$

Because the small or large $g\lambda$, the first stream lane flows very slow or fast and the width of the first stream lane become wider or narrower. At the fixed the post array with the fixed gap and shift fraction, the critical radius of the particle is determined. As shown figure 2-3(c), the large cell like CTC travels the micro scale array as the bumping mode and the small cell such as WBC and RBC flow the micro pillar array as the zigzag mode. Based on the size of the cells, the trajectories of the targeted large cells and small cells are different and there are separated. Loutherback's group [117] designed the triangular post array to separate breast cancer cells from the spiked blood sample. The gap size of this system was 42 μm and the sift row fraction was 1/20. The blood sample was dilute between 5 to 20 times and the breast cancer cells (MCF10A and malignant MDAMB231) were used as approximately 10^7cells/ml to added to the 500 $\mu\ell$ of the blood sample and the sample was diluted to the total volume the sample was 10mL. In the experiment, MCF10A cells were separated to collect outlet with the capture efficiency of 91% at flow rate 500 $\mu\ell$/min and the malignant MDAMB231 cells were separated to collect outlet with the capture efficiency greater than 85% at flow rate 10mL/min, respectively [117]. The cell viability of MCF10A cells was higher than 96% with different flow rate 0.5, 5.0, 10mL/min and especially the cell viability

of MCF10A cells at 5.0mL/min flow rate is 100%. Using DLD system, the CTCs were separated by the larger size than the other blood cells. Moreover DLD device could offer the high throughput and the cell viability after the isolation process is almost 100%. The intact blood sample was used 500 ㎕, but the number of CTCs (10^7 cells/mL) in the final sample was higher than compared to the blood cells (leukocytes) in the experiment. In result, the average cell size was 19.5 ㎛ in the inlet and the collection outlet and 19 ㎛ in the waste outlet. The number of CTCs was not similar to the real number of CTCs of blood sampled derived from the cancer patient, so additional experiment is needed using the blood sample with the similar cell composition. Moreover the capture efficiency was lower than other microfluidic device, missing CTCs means the missing the information source. It can affect to the molecular analysis after the separation process.

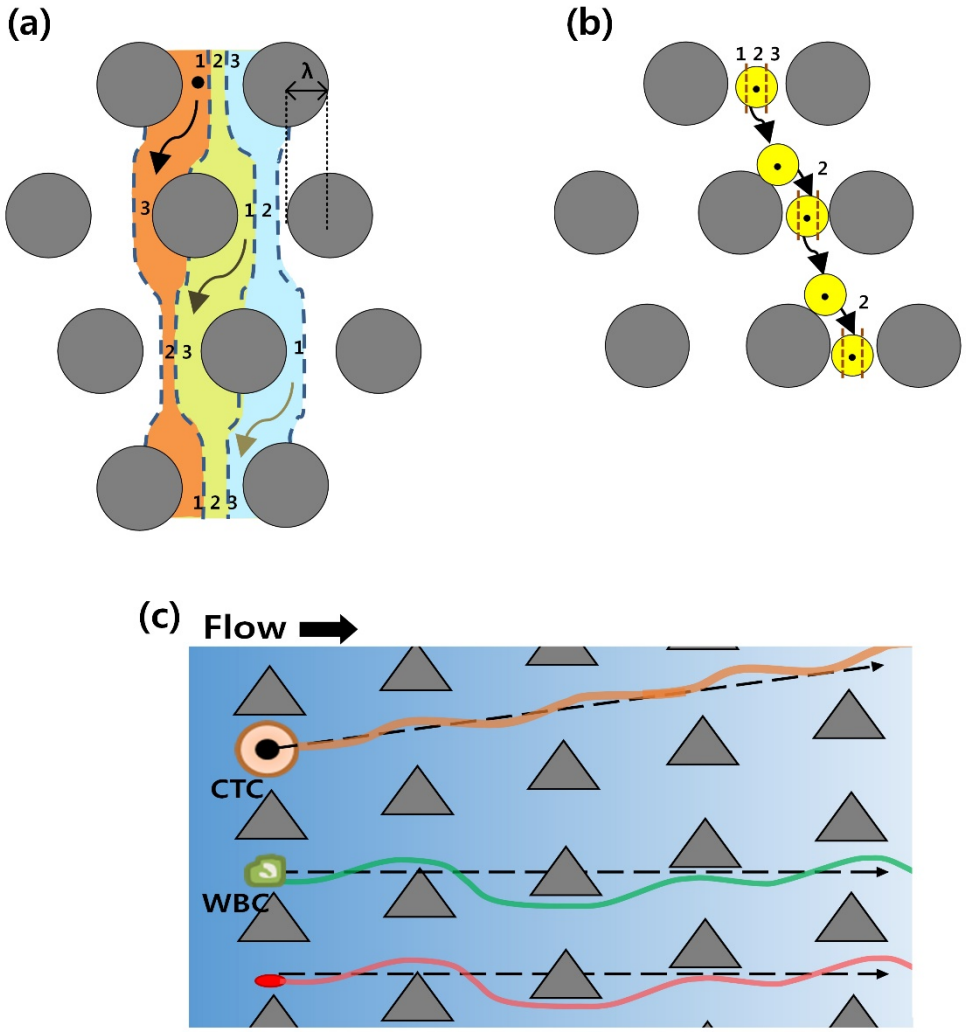

Fig 2-3. The principle of DLD and the trajectories of three types of cells. (a) When the micro pillars are regularly shifted the flow lanes are divided with the shifted rate, λ. Small size of cell flows through the shifted micro pillar array through specific stream lane and the direction of cell is same to an initial position. (b) Large size of cell flows with bumping and the direction of this cell becomes more distant from the initial position. (c) Shifted micro pillar are arranged and the fluid flow from left to right. In the microfluidic channel, large cell (CTC), middle size cell (WBC) and small cell (RBC) flow to different direction.

Other separation principle is to make the curved microchannel and the different size particles experience the different centrifugal force in this curved microchannel. In the curved micro scale channel, the fluid are divided two portion and the direction of the fluid flowing is clockwise and counter clockwise. Because the fluid velocity profile is twisted from the inner to outer of bending as the peak velocity moves to the outside, the fluid, which is closer to the inner site of the bending, is pushed to outer wall [118]. The fluid at the outer wall side flows back to the inner bending site along the wall. Based on the horizontal axis at the center of fluid flowing, the up-portion of fluid forms the count clock vortex and the down-portion of fluid forms the clock vortex. This vortex is called Dean's vortex or Dean's flow [119, 120]. The Dean's flow effect is determined by the dimensionless number Dean number (κ) [118, 120, 121], which are described as

$$\kappa = \delta^{0.5} Re \tag{1.20}$$

where δ is the ratio between the width of the microchannel and the radius of the curvature. When the different fluids flow the curvilinear channel with the high κ, the fluids well generated vortexes and they can change their position. With low κ, the fluids cannot mix. Initially this phenomena has been studying about mixing in the meander shape microfluidic system [121-124], but when the multi-size particles are included, these particles experience the inertial lift force (F_L) [100, 125] and the Dean drag force ($F_{D,d}$). F_L, which is induced by the shear rate, pushes the particle from the wall to the center line in the fluid and $F_{D,d}$, which is assumed from the Stokes drag, drives the particle to follow the Dean vortex with proportional to the Dean velocity (U_{Dean}) [125-127]. Two vortexes of fluid are generated in the bending channel and the particle experiences the two types of forces. As shown figure 2-4(a), when the particle flows near the top and bottom wall sides (position3

and 4), the $F_{D,d}$ only affects to the particle to move inner wall or outer wall. But when the particle flows at the inner or outer wall (position1 and 2), the particle experiences the gap force between the F_L and $F_{D,d}$ and it is focused to equilibrium position because F_L and $F_{D,d}$ act to reverse direction. These forces and the Dean velocity are expressed as

$$F_L = \rho\left(\frac{U_m}{D_h}\right)^2 C_L a^4 \tag{1.21}$$

$$F_{D,d} = 3\pi\mu U_{Dean} a \tag{1.22}$$

$$U_{Dean} = 1.8 \times 10^{-4} \kappa^{1.63} \tag{1.23}$$

where, ρ is a fluid density and C_L is the coefficient related to the position of the particle in the cross-section of the microchannel assuming as 0.5 [125, 128]. U_{Dean} affects to $F_{D,d}$ to drive the particle. Because the F_L is proportional to $a^4$and $F_{D,d}$ is proportional to a, two forces significantly depend on the particle size and the equilibrium of tow forces determines the different focusing position. Therefore the different sized particles are separated by different equilibrium position. Han Wei Hou's group [129] designed Dean flow fractionation (DFF) to separate CTCs using the Dean flow. Figure 2-4 shows the DFF system. To demonstrate DFF system, they used the MCF-7 cells (~10^5 cells/mL) spiked 20% hematocrit whole blood sample and sheath buffer were injected with ratio of 1:9 to push the cells to near the outer inlet. In term of the Dean Cycle (DC), the lateral migration of the particle was described. As figure 2-4(b), when the cells were entered and the cells flown along the outer inlet because the cells were not experience any force, as cross-section view of X position. When the cells flown downstream forward to 1/2 DC, they focused at inner wall side by acing of $F_{D,d}$, like a cross-section view of Y position. Finally the blood cells were focused to the outer outlet due to $F_{D,d}$, but CTCs were focused at the inner outlet, at

the cross-sectional sight of Z position. Because the size of CTCs is larger than the blood cells, F_L affects weakly to the blood cells and this force affects strongly to CTCs. Therefore the focusing position of CTCs is inner outlet and the focusing position of the blood cells is outer outlet due to the different magnitude of the inertial lift force. In result, the capture efficiency of this system was greater than 85% [129]. Some of rare CTCs were missed because the similar size of leukocyte and the undesired cell-cell interaction in the DFF system while the flowing. To prevent the interference of the undesired blood cells in the CTC collect outlet, they used two stages of DFF system and the enrichment ratio between the cancer cells over RBC about 10^9 fold and over leukocyte ~10^3 fold at the end of the second stage. It meant the possibility of blood cell removal, but the initial number of the cancer cell in the used sample was very higher than real number of CTCs and the enrichment should be high.

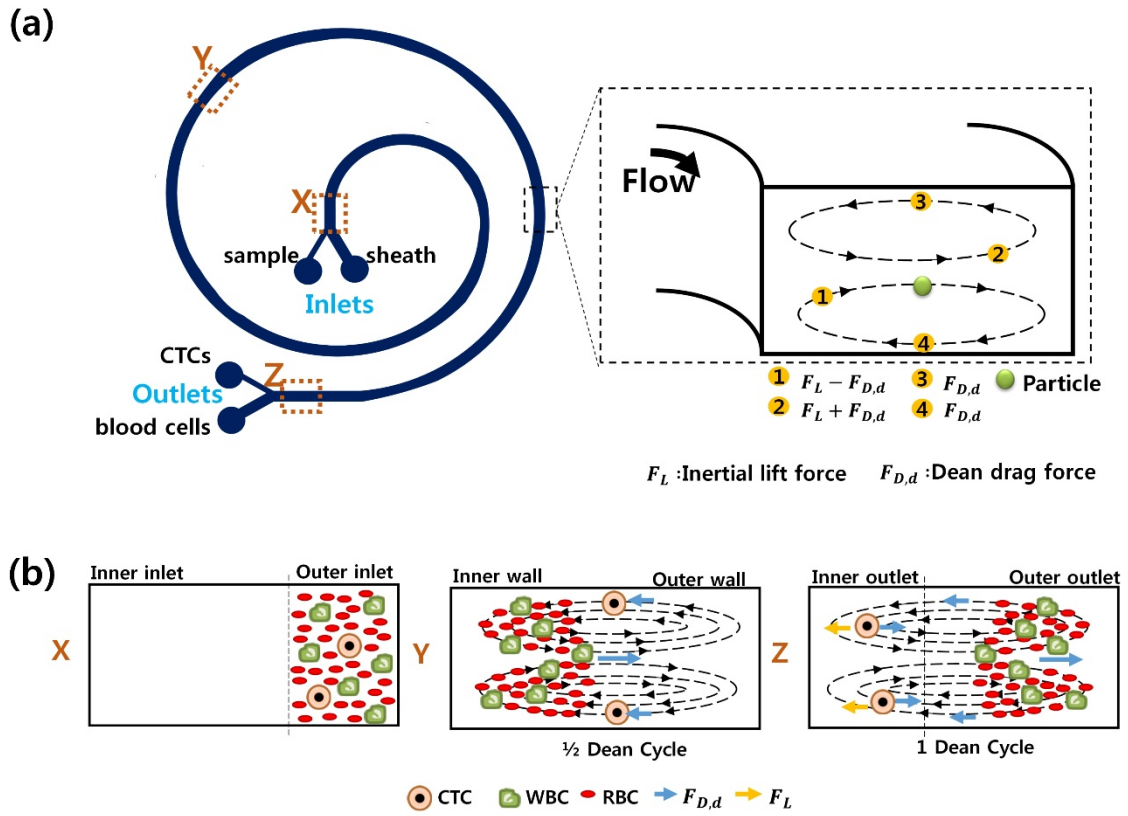

Figure 2-4. The principle of DFF system in view of the cross-sectional. (a)When the particle flow in the curvature microchannel, the particle flows along the Dean's flow and it experiences two types of forces F_L and $F_{D,d}$. The balance between two forces, the flowing position of particle is decided. When the CTCs, leukocytes and RBCs enter to the microchannel through the sample inlet, all cells flow outer inlet at the X stage. At Y stage (it is called 1/2 Dean Cycle), CTCs and leukocytes and RBCs are flow forward inner wall by $F_{D,d}$. At Z stage (it is called 1 Dean Cycle), CTCs only focus to inner outlet. By the different force equilibrium, the blood cells and CTCs are separated to outer outlet and inner outlet, respectively.

They all are the size based separation methods under the different hydrodynamic principle. Using the evaluate parameters, these diverse system can provide the high capture efficiency and the high throughput. Among the size based microfluidic separation technologies, MS-MOFF offers the highest capture efficiency 98.9% and DLD provides the highest capture purity 16.7%, as the summary is shown table2. Despite of the near 100% of capture efficiency of MS-MOFF, the percentage of the non-targeted blood cells is 97.9% at the collect outlet. Also the 16.7% of the capture purity of DLD system is the highest result, but it is not enough for the accurate molecular analysis and the capture efficiency of DLD is greater the 85%, which is lower than other microfluidic system.

Device type	Target cells	Purity (%)	Efficiency (%)	Inlet flow rate (㎕/min)
MOFF	MCF-7	1.5	88.8	100-300
MS-MOFF	MCF-7	0.3	98.9	108-144
p-MOFF	MCF-7 BDA-MB-231	-	93.75 91.60	600
DLD	MDA-MB-231	16.7	>85	500
DFF	MCF-7 HeLa MDA-MB-231	-	>85	500

Table 2. The overviews of the sized based separation microfluidic device.

1.4 Limitation and Hypothesis

The size based hydrodynamic size based separation technology offers the high capture efficiency as the series of MOFF system the capture purity is comparatively low. As mentioned before, the capture purity parameter means how the undesired blood cells are removed from the mixture blood sample and the isolated CTC outlet, this parameter is important to the subsequent phenotypic and genotypic analyses about the isolated CTCs [130]. So, a number of the unremoved blood cells in the collected CTC outlet may interferences the molecular analysis and make the variation to the result of the analysis. The variable result can affect to the diagnosis or the cancer treatment to the physician and the patient, and the development of the drugs or biomarker. To keep the high capture efficiency of the size based separation technology and enhance the capture purity, other approach is required to analyze the reason of the low purity and reduce the huge number of the blood cells in the collect outlet. The why the undesired blood cells disturb to the isolation of CTCs has been studying as the similar or same size of the blood cells and CTCs. The sight about the size overlapping between the blood cells and CTCs is previously used to interpret and analyze the low capture purity. However, this sight is limited to describe the experimental results about the low capture purity and understand the reason about the interference of a number of the non-targeted cells. Additional sight is required to more accurate and real interpret the phenomenon in the size based separation microfluidics and increase the capture purity. The cell deformability is needed to describe and enhance the low capture purity of size based separation technology. Because in the microfluidic system, which based on the size difference between the targeted cells and non-targeted cells, the two kind of the cells actually experience the forces acting to the cells and the cells can deform while the cells flow to be

separated.

In this study, the cell deformability parameter is used to reflect the real cell properties and suggest the new approach for the analysis of the reason to the low capture purity of MOFF series and understand the effects of the cell deformability. Using COMSOL simulation tool, the rigid particle and deformable particle are characterized with different values of the deformability. By applying the cell deformability parameter and putting on other parameters as same, the trajectories and focusing positions of the multi-size particles will be observed and interpreted. Also the particles behavior will be observed with inlet fluid velocity change.

2. MATERIALS AND METHODS

2.1 Theoretical fundamentals

The theoretical fundamentals of the microfluidic system is based on the interaction between the fluid flow and the solid mechanics. The principle of this phenomena in the designed microfluidic device is governed by using the Navier-Stokes equations [131, 132] for fluid flow, the Newtonian formulation [132, 133] for the particle tracing, the equation of linear elastodynamics for the solid mechanics [132, 134] for particle deformability, and the fluid-solid interaction (FSI) for the effects on the particles and fluid each other.

2.1.1 Fluid flow

In the microfluidic environment, the behavior of the fluid is governed by the Navier-Stokes equations [131, 132]. The fluid is an incompressible flow and the Reynolds number of this fluid is very small since the small dimensions of the microchannel. The governing equation of laminar flow is shown at equation from (2.1) to (2.3).

$$\rho_f \frac{\partial u_f}{\partial t} + \rho_f (u_f \cdot \nabla) u_f = \nabla \cdot \left[-p_f I + u_f \left(\nabla u_f + (\nabla u_f)^T \right) \right] - 12 \frac{\mu_f u_f}{H^2} + F_f \quad (2.1)$$

$$-12 \frac{\mu_f u_f}{H^2} = F_H \quad (2.2)$$

$$\rho_f \nabla \cdot u_f = 0 \quad (2.3)$$

Where ρ_f is the density of the fluid, $u_f = (u_f, v_f, w_f)$ is the local velocity of the fluid, t is the time, ∇ is the gradient operator, p_f is the pressure of the fluid, I is the identity matrix, μ_f is the dynamic viscosity of the fluid, H is the channel height, F_H is the

drag term as a volume force, which is added by the shallow channel approximation for correct calculation [131, 132], F_f is the pressure-driven volume force to the fluid flow and $\nabla \cdot$ is the divergence operator. The fluid flow is determined by the pressure of the fluid and the viscosity of the fluid. The left term describes the velocity term of the fluid, the first part is local acceleration and the second part is a convective acceleration of the fluid. The pressure term at the right has negative value as the pressure of the fluid decreases along the direction of fluid flowing. The shear stress term at the right is generated by the fluid viscosity. At the final term of the right part the drag force term, which is formed by the effect of the shallow channel approximation and it is used to more similar to the real microfluidic device environment, and the volume force act on the fluid. The equation (2.3) is the term of the convective acceleration, it can be neglected since the incompressible flow has the constant density.

2.1.2 Solid mechanics

The solid particle can displace and deform with the linear elastodynamics [132, 134] in compared to the particle tracing physics. Because the parameters that is related to the Young's modulus and the Poisson's ratio of the particle, the behavior of solid particle can be described.

The governing equations are described as

$$\nabla \cdot \sigma_s + F_s = \rho_s \frac{\partial^2 u_s}{\partial^2 t} \tag{2.5}$$

$$\sigma_s = C\varepsilon_s \tag{2.6}$$

$$\varepsilon_s = \frac{1}{2}[(\nabla u_s)^T + \nabla u_s + (\nabla u_s)^T \nabla u_s] \tag{2.7}$$

where σ_s is the particle Cauchy stress tensor [135], which is simply called by the stress tensor and it is used to stress analysis of material body, F_s is the volume force affecting the particle, $u_s = (u_s, v_s, w_s)$ is the displacement field of the solid, ρ_s is the density of the solid, C is the stiffness matrix and ε_s is the infinitesimal strain tensor [136], which explains the deformation of a solid. The equation (2.5) is derived from the Newton's equation of motion, the displacement of the particle is denoted. The equation (2.6) is the linear elastic stress-strain relation in proportional to the C, the deformability of the solid particle is defined by this equation. The C is defined with the Young's modulus and Poisson ratio of the solid, this stiffness matrix is used to solve the displacement, stress and strain value. The equation (2.7) is the strain-displacement equation, the strain of the particle can be described by the displacement of the particle.

2.1.3 Fluid-solid interaction (FSI)

The fluid flow and the solid mechanics are coupled as FSI, to describe the interaction between the fluid flow and the solid in the fluidic condition. The fluid affects to on the solid particle and the particle moves with the load of the suspending fluid, especially the solid particle can change its shape with the Young's modulus and the Poisson's ratio. Also the particle can affect to the fluid flow, the velocity or the fluid flux can be changed with the displacement or location of the particle. The relationship between the fluid flow and the solid mechanics is described as

$$f_s = -n \cdot \left[-p_f I + \mu_f \left(\nabla \mu_f + \left(\nabla \mu_f\right)^T\right)\right] \tag{2.8}$$

$$u_w = \frac{\partial u_s}{\partial t}, \quad u_f = u_w \tag{2.9}$$

where n is the outer normal to the boundary, the force F_s can be transformed to the f_s and u_w is the rate of change between the displacement of t0he solid. The pressure and the viscous force of the fluid exerts on the solid particle and the deformed and displaced particle affects to the fluid flow as equation (2.8). The change ratio of the particle movement is equal to the fluid velocity at the fluid-solid boundary as equation (2.9), this means the solid boundary acts as a non-slip wall for the fluid domain.

2.2 Design and simulation

The microfluidic system is described as figure 3-1. We designed three types of microfluidic device as the original MOFF, the compacted MOFF system to enhance the shear rate on the deformable particle in the shorter channel dimension (length and width) than MOFF, and the expansion area at the end of the MOFF system for the final separation is divided as the individual simulation model. Using the compacted design with the shorter channel and divided model, the calculation time can be saved. Like the MOFF system, the compacted MOFF system and the divided expansion model have one inlet and outlet, the compacted MOFF has the contraction/expansion area. The particle diameter is equal under the particle tracing physics and the FSI physics to observe the trajectory of the particle in the microfluidic system by except the effect of the size difference and only consider the particle deformability.

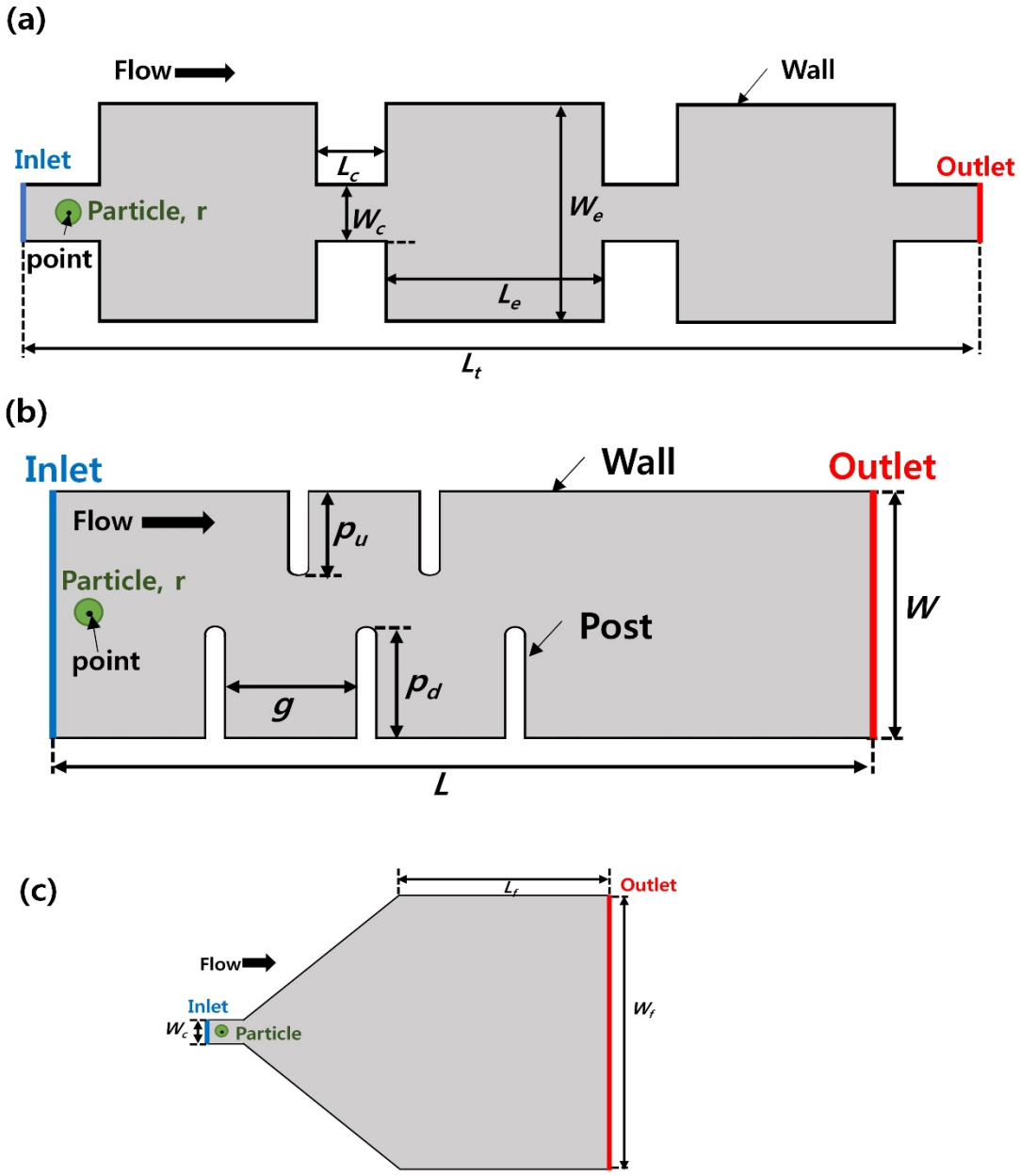

Figure 3-1. The simulation models are illustrated. There are (a) single stage MOFF model, (b) compacted MOFF model and (c) the final expansion chamber of MOFF model. All the model, the fluid are suspending in the microfluidic system and the particle is driven by the fluid. The point on the center of the particle is used as the standard point to describe the particle trajectory. The trajectory of the particle determined in the channel. The fluid flows from the left inlet to the right outlet. Each values for the channel dimension and the particle size are given at the table3.

Parameter	Value
L_c (contraction channel length)	100 ㎛
L_e (expansion channel length)	200 ㎛
L_t (total channel length of MOFF)	1000 ㎛
W_c (contraction channel width)	40 ㎛
W_e (expansion channel width)	120 ㎛
g (gap between posts)	46 ㎛
P_u (upside post height)	27 ㎛
P_d (downside post height)	25 ㎛
L (channel length of compacted MOFF)	250 ㎛
W (channel width of compacted MOFF)	45 ㎛
L_f (final expansion channel length)	600 ㎛
W_f (final expansion channel width)	800 ㎛
μ_f (viscosity of fluid)	0.001 Pa·s
ρ_f (density of fluid)	1000 kg/㎥
ρ_1 (density of rigid particle)	1050 kg/㎥
ρ_2 (density of stiff particle)	1050 kg/㎥
ρ_3 (density of soft particle)	1050 kg/㎥
P_1 (Poisson ratio of rigid particle)	0.4
P_2 (Poisson ratio of stiff particle)	1e-8
P_3 (Poisson ratio of soft particle)	1e-9
E_1 (Young's modulus of rigid particle)	1 kPa
E_2 (Young's modulus of stiff particle)	0.1 kPa
E_3 (Young's modulus of soft particle)	1 MPa
H (channel height)	50 ㎛
r (particle diameter)	5 ㎛

Table3. The given simulation parameters

The fluid enters to the microchannel through the inlet and the fluid flows from the inlet to the outlet by the gradient of fluid pressure. The fluid velocity profile at the inlet is parabolic shape and it is defined at the equation (2.10).

$$\mathrm{U} = u_0 \frac{6(W-Y)Y}{W^2} f_{step} \tag{2.10}$$

Where U is the inflow velocity profile as the parabolic profile, u_0 is the given fluid velocity, f_{step} is the step function for the smooth inflow, W and Y is the width of the inlet and the material frame coordinate along the inlet, respectively. When the particle tracing module, the mean velocity is equally applied to the inflow velocity profile.

At the outlet, the boundary condition is defined as equation (2.11). The fluid pressure and the viscous force of the fluid are zero.

$$p_f = 0, \quad \mu_f\left(\nabla\mu_f + (\nabla\mu_f)^T\right)n = 0 \tag{2.11}$$

The wall condition is the no-slip condition, so the fluid velocity at the wall side is zero as shown equation (2.12).

$$u_f\big|_w = 0 \tag{2.12}$$

In the particle tracing modules, the wall condition is bounce and the outlet condition is freeze. If the particle strikes the wall or the outlet, the particle is bounced from the walls or attached to the outlet.

The frame of fluid and the particle will be defined by the arbitrary Lagrangian-Eulerian (ALE) [132, 137], because the behavior and the interaction between the fluid flow and the particles continuously freely move and deform. This method can describe the current configuration of the spatial frame and the material frame along the solid particle displacement and the state of the deformability. The re-meshing operation stops the simulation and destroys the mesh mapping to create a new mesh related to the current

arrange and the position of frame. To describe the interface between the fluid domain and the solid particle domain, ALE method is used. The mesh is to divide the simulation models to the finite number of the elements for calculating. The mesh element size of the fluid dynamics is predefined as finer and those of the general physics is predefined as normal. The meshing of the general physics is referenced by the meshing of the fluid dynamics. The mesh smoothing type is defined as the hyperelastic to describe the deformable particle like as blood cells.

The simulation will be processed with the critical boundary conditions and the result will be changed with the given different conditions. The FSI will be used to calculate the several types of particle trajectories in the MOFF model and the compacted MOFF model with the different fluid velocity and original location of particle. The different characterized particles are modeled as rigid particle, stiff particle, which is modeling of cancer cell, and soft particle, which is modeling of normal blood cell like a leukocyte.

3. Results and Discussion

3.1 Rigid particle and deformable particle in MOFF

Three types of the particle, which size is commonly 10 ㎛, moves in MOFF model and the trajectories of particle are calculated. First particle is a rigid particle, and this rigid particle has the value of Young's modulus and the Poisson ratio are 1MPa and 0.4, respectively. Second particle is a stiff particle, which particle is modeled as cancer cell, and the Young's modulus and the Poisson ratio of this particle are 1kPa and 1e-8, respectively. Third particle is a soft particle, which particle is modeled as normal blood cell like a leukocyte, and the Young's modulus and the Poisson ratio of this particle are 0.1kPa and 1e-9, respectively. Theses Young's modulus value of deformable particles is derived from the previous experimental results [77, 78]. The given original locations of particle are the center of the inlet microchannel and upper 5 ㎛ from the center. The trajectory of particle is described to base on the central point of particle. The fluid velocity is given as 10mm/s and the maximum fluid velocities of different case are similar.

Shown as figure 4-1, each maximum fluid velocities are 2942.9 ㎛/s, 2942.4 ㎛/s and 2942.6 ㎛/s, and the trajectory of rigid particle is different from those of deformable particles. The rigid particle travels as shown figure 4-1(a), the particle trajectory is gradually downward from the beginning expansion area to final expansion area and each peak y-position at each expansion area are upper than 0 ㎛. The minimum y-component is -28.798 ㎛ and the final y-position of this particle is 2.134 ㎛ from the baseline as initial y-position of rigid particle. But the deformable particle trajectories shows comparable shape like figure 4-1(b) and (c). In first expansion area, the stiff particle and soft particle flow

slightly down-direction from original y-component as -0.308 ㎛ and -0.926 ㎛. These deformable particles move up-direction with compared to the case at first expansion area. The maximum y-component and the final y-component of stiff particle and soft particle are 1.094 ㎛ and 0.517 ㎛, and 0.836 ㎛ and 0.378 ㎛. As results, the trajectories and focusing position of rigid particle and deformable particles are different under the similar fluid velocity. The deformability property of particle affects to the particle displacement at the similar fluid velocity. Start at the centerline, the deformable particles are focused on the near the centerline with compared to the rigid particle focusing position and the final position gap between the rigid particle and deformable particle increase along the stage of MOFF model. The focusing position gap between the stiff and soft particle is little. Despite of there is probability to the gap increases, the increasing rate is also subtle. Therefore, the soft particle is isolated to same position with the stiff particle and it is why of the low capture purity.

Figure 4-2. shows the result of several velocity magnitude field and displacement field of applied particles at the beside of centerline. Under the same boundary condition of figure 4-1, these particles are located at 5 ㎛ upper than the center of inlet microchannel. Also the inflow velocity is 10mm/s and each maximum fluid velocities are 2941.7 ㎛/s, 2943.3 ㎛/s and 2944.1 ㎛/s. Compared to the displacement of center located particles, all type of particles, which are located to beside of the centerline, travels the comparable route. From beginning to the end of model, all particle move meandering each expansion area. So the y component of all particle gradually upper from the initial y component and the final focusing y position of several particles are different. In result, the maximum position of rigid, stiff and soft particle are 31.539 ㎛, 38.284 ㎛ and 37.882 ㎛, respectively. The deformable particles tend to spread out to the expansion area and its maximum y position is upper from the initial

y position than the rigid particle. The final focusing y component of rigid, stiff and soft particle are 2.134 ㎛, 4.029 ㎛ and 3.848 ㎛, respectively. The rigid particle is focused to the lowest position compared with the deformable particles. Like an above result of, the deformability parameter affects to the particle focusing position and trajectory. The final focusing y position between the stiff and soft particle is subtle, so the stiff and soft particles move to same route. Therefore the capture purity decreases by the same separation position of stiff and soft particle.

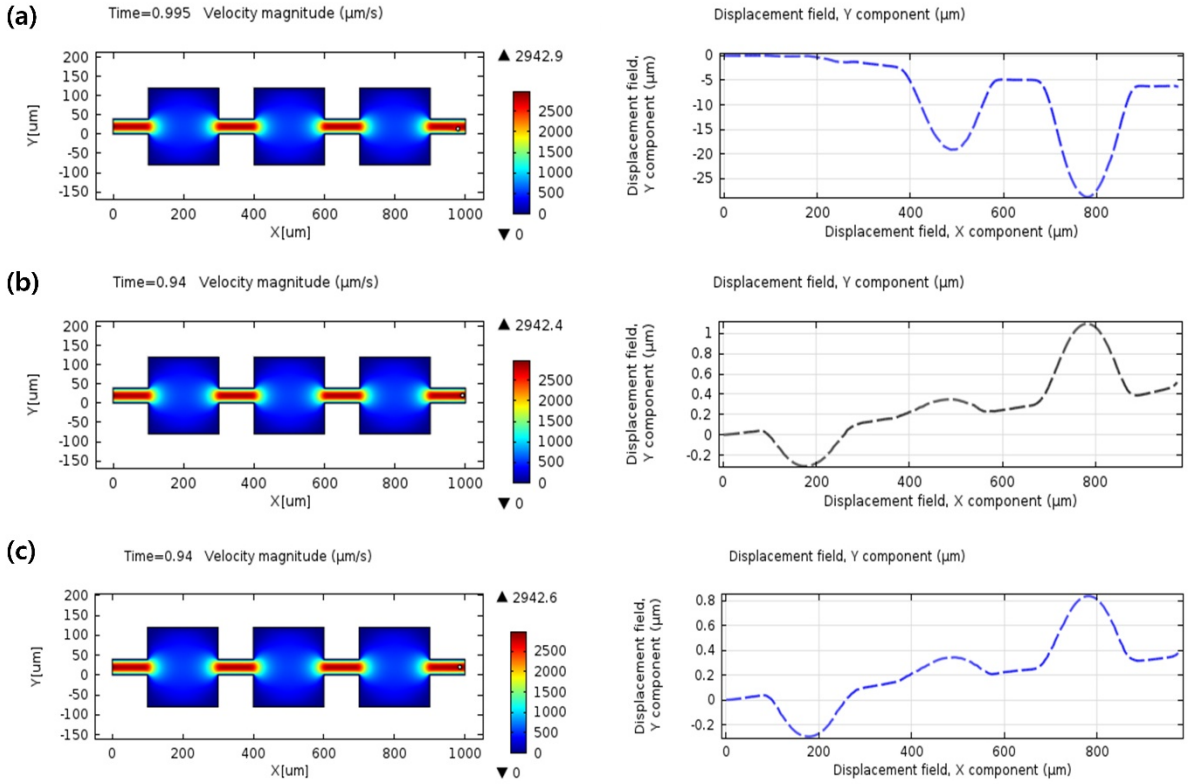

Figure 4-1. The velocity magnitude field and three type of particles displacement filed are shown. The left figure is velocity field of the microfluidic system. The right graph describes the displacement of the particle on the x-y plane with basic the y component of initial position as zero. The fluid are input with particle at given fluid velocity and particle position. The x-axis and the y-axis show spatial frame and the unit is ㎛. The red color and blue color in the velocity field are a high and low fluid velocity with unit of ㎛/s. (a) A rigid particle displacement tends to go down forward and the final y-position of this particle is lower than the initial y-position. The trajectories of (b) stiff particle and (c) soft particle show a similar pattern. Two particles somewhat flow down direction at first expansion area, but these particles move gradually upper direction at second and third expansion area. The final y-component of the stiff particle is slightly upper than those of soft particle.

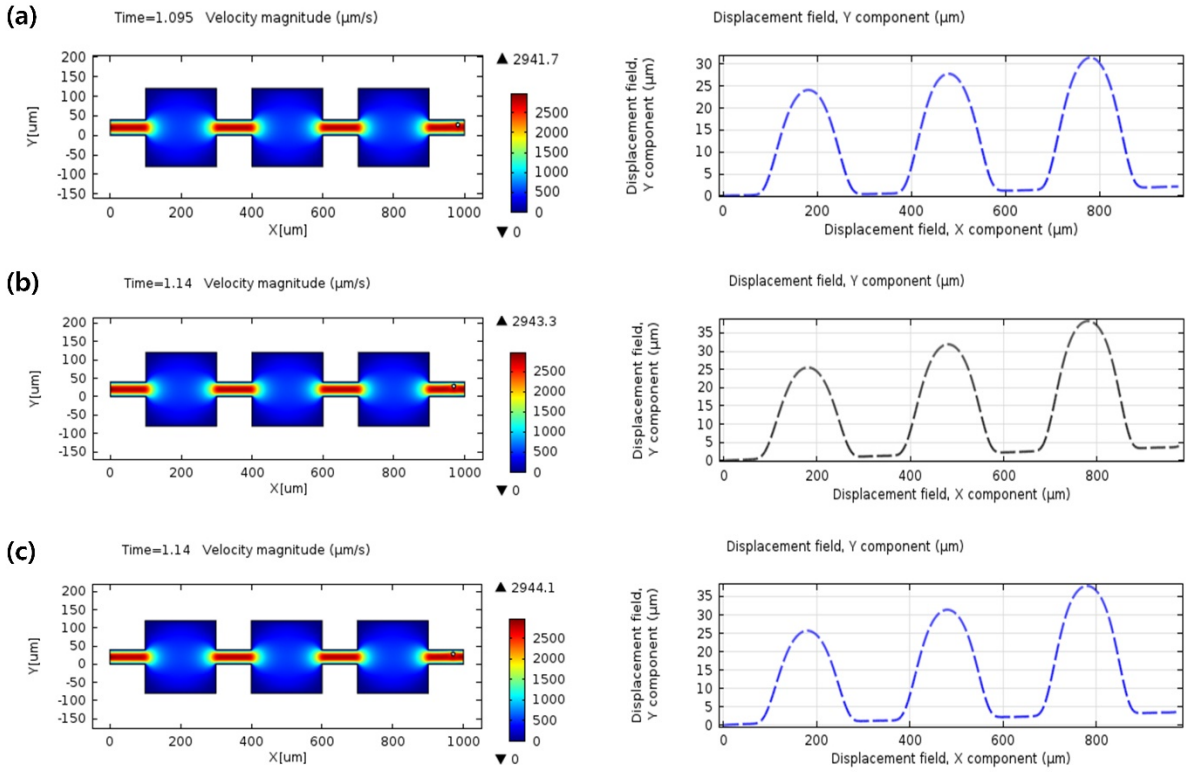

Figure 4-2. The velocity magnitude field and three type of particles displacement filed are shown as (a) the rigid particle (b) the stiff particle (c) the soft particle. The fluid are input with particle at given fluid velocity and particle is initially located to slightly distant site from the center position of the inlet microchannel. The trajectories of three particles are similar to each other, but the trajectory of the rigid particle is slightly different from the other two particles. The each peak y-position of rigid particle in MOFF model is lower than those of the deformable particles. Also the travelling time of rigid particle is shorter than those of the deformable particles.

3.2 Comparison MOFF and compacted MOFF

The stiff particle displaces in the model of MOFF and the compacted MOFF. The governing physics is FSI, the fluid velocity of MOFF model is 10mm/s and those of compacted MOFF model is 900 ㎛/s. The particle, which is 10 ㎛ size, has the deformability property as stiff particle. In result, the particle is focused to different position after the contraction and expansion area. The maximum fluid velocity at the MOFF and the compacted MOFF model are similar as 2942.3 ㎛/s and 2972.6 ㎛/s, respectively. The fluid velocity is maximum at the contraction area in both of MOFF and compacted MOFF. As figure 4-3(a), the particle position is higher than the previous orifice shaped chamber. The initial particle position is standard to zero at the start point of MOFF model and the particle position after the two stage MOFF increases to 4.029 ㎛. In the compacted MOFF model figure 4-3(b), the particle is focused to the lower position than the initial position as decreased to -13.655 ㎛. The difference between the initial particle location and equilibrium location is larger at the compacted MOFF model than the original MOFF model. By decreasing the microchannel dimension, the calculating time can be shorten and the applied particle experiences the additional forces.

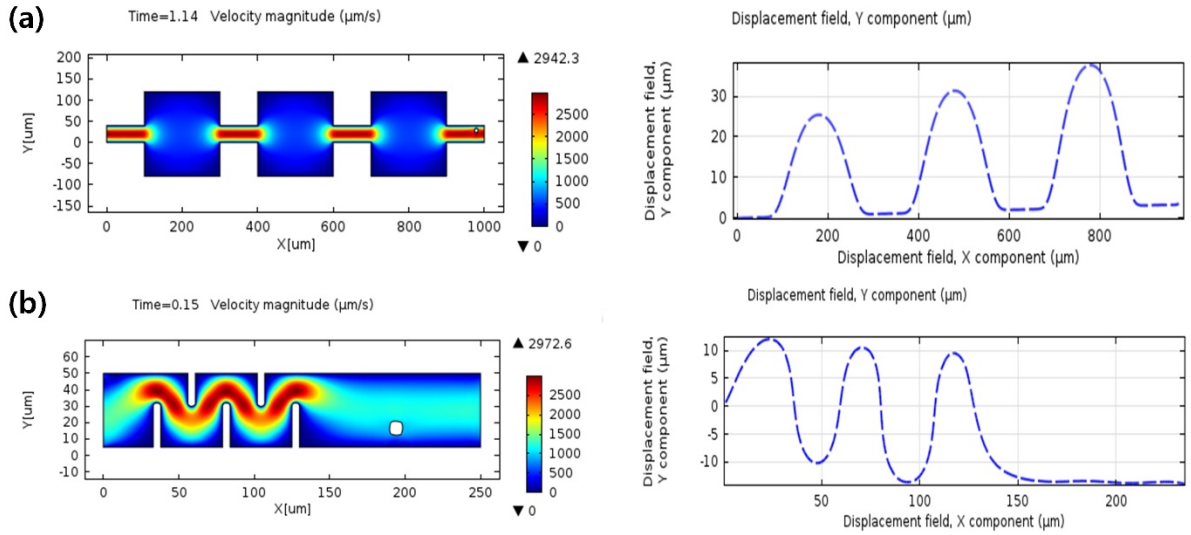

Figure 4-3. The velocity field and the stiff particle displacement field are illustrated. (a) It shows the velocity field at the time as 1.14s and the particle displacement field of the MOFF model. The position of particle is changed through the MOFF stage to higher than the initial position. (b) It shows the velocity field at the time as 0.14s and the particle displacement field of the compacted MOFF model. The position of particle is lower than the initial position to near the wall side.

3.3 Particle trajectory in compacted MOFF

When the deformability property is differently applied to the particle, the trajectory of the particle is affected by the force of the fluid flow and the particle deformability affects to the fluid flow. The interaction between the rigid and deformable particle, and the fluid flow is calculated by using the FSI physics. So, the deformability parameters of the particle, which are defined by the Young's modulus and the Poisson's ratio, is applied to generate the difference between the rigid particle, stiff particle and soft particle. The initial position of three particles is same as the calibrated position, zero. Under the same boundary condition without the particle deformability parameter, the different particles move to their focusing position by the interaction between the particle and the fluid in the microchannel. Another parameter acting to the trajectory of the particle is the fluid velocity, the several fluid velocity condition is applied in the compacted MOFF model. The different inflow fluid velocities act to the same particle and the particle trajectories with the different fluid velocity are defined by the interaction with fluid and the solid particle. The fluid velocity magnitude field and the displacement of particle at the channel are described each sections. The velocity magnitude expressions the special simulation time to compare the position of each particles along the deformability parameter. The displacement field of three particles are described from 0㎛ to 230㎛.

3.3.1 Focusing position with different deformability

When the deformability parameters are applied to the particle, the behavior of the particle is different from the non-deformable particle. From the figure 4-4 to figure 4-6, the particles with different amount of deformability travel in the compacted MOFF model and the particles are focused to their each position. At the three figures, (a) group shows the case of the rigid particle, (b) group shows the case of the stiff particle and (c) group shows the case of the soft particle. As shown figure 4-4, the given initial fluid velocity is 300㎛/s and the maximum fluid velocities of three simulation result are 991.05㎛/s, 990.78㎛/s and 991.2 ㎛/s, respectively. At the same simulation time as 0.35s, the x-axial position of particles are similar as 181㎛. In result, the rigid particle, stiff particle and soft particle are finally focused to -3.341㎛, -2.234㎛ and -3.433㎛, respectively. The rigid particle and soft particle are focused to similar y-position with 0.092㎛ of gap and the stiff particle is focused to upper position than the rigid and soft particle. As shown figure 4-5, the given initial fluid velocity is 600㎛/s and the maximum fluid velocities of three simulation results are 1983.1㎛/s, 1981.7㎛/s and 1981.3㎛/s, respectively. At the same simulation time as 0.2s, the stiff particle moves above than 200㎛ and other particles need more time to pass the 200㎛ point. The final focusing y-position of three particles at the 230㎛ on x axis are -5.099㎛ to rigid particle, -6.031㎛ to stiff particle and -12.071㎛ to soft particle. The lowest focusing y-position of applied particle is -12.071㎛ to soft particle. The gap between y-positions of rigid and stiff particle is small as 1㎛, but the soft particle is distinctly focused to low position than other particle. The y-position becomes be low along the increased deformability of particle. As shown figure 4-6, the fixed initial fluid velocity is 900㎛/s and

the maximum fluid velocities of three simulation result are 2970.3㎛/s, 2972.5㎛/s and 2971.8㎛/s, respectively. The rigid particle and soft particle pass the 200㎛ point at simulation time as 0.15s and the stiff particle only lags behind the 200㎛ point. On the 230 ㎛ of horizontal axis, the rigid, stiff and soft particles are finally focused to -1.057㎛, -13.655㎛ and -13.655㎛, respectively. The rigid particle only near to the initial y-position with 1.057㎛ of gap, but the deformable particles are focused to considerably low position than the initial location. In compared to the rigid particle, the deformable particles are focused to same y-position and this distance is 13times than those of rigid particle. The rigid and deformable particles move with similar trajectory in the contraction area of the microchannel, but they are differently focused to their each final position. The applied deformability of particle affects to the particle trajectory and the displacement of particle changes from the case of the rigid particle at the same fluid velocity. The deformability of particle should be considered to correct analysis of the separation effect and enhance the capture purity.

3.3.2 Focusing position with different fluid velocity

With different fluid velocity, the rigid and deformable particles travel to different way. Other condition about the properties of the particles and the boundary condition are fixed, only the fluid velocity is differently applied. The fluid velocity affects to the trajectory of the particle and the focusing positon is different with the fluid velocity. The fluid with 300, 600 and 900 ㎛/s is applied with the particle, the trajectory of the particle is described from figure 4-4 to figure 4-6. The time to simulation becomes short along the increased applied fluid velocity and the particles early reach to the ending wall. The rigid, stiff and soft particle are compared with the final focusing y-position in order. The different particles are commonly focused to lower position than the initial position and the distance from the initial position tends to increase along the increased applied fluid velocity. But, the focusing position of rigid particle decreases when the inlet fluid velocity is 900 ㎛/s. The final focusing y-position increases from the 300 ㎛/s to 600 ㎛/s with 1.758 ㎛ of gap and it decreases from the 600 ㎛/s to 900 ㎛/s with 4.042 ㎛ of gap. The focusing position when the fluid velocity 900 ㎛/s is smaller than the focusing position when the fluid velocity 300 ㎛/s. In case of stiff particle, the final focusing y-position increases from the 300 ㎛/s to 600 ㎛/s with 3.799 ㎛ of gap and from the 600 ㎛/s to 900 ㎛/s with 7.624 ㎛ of gap. Other case of soft particle, the final focusing y-position increases from the 300 ㎛/s to 600 ㎛/s with 8.693 ㎛ of gap and from the 600 ㎛/s to 900 ㎛/s with 1.584 ㎛ of gap. When the applied fluid velocity increases, the force, which is induced by the fluid flowing, affects strongly to the particle. By increased fluid induced force, the particle experiences trajectory change. In compared to the rigid particle, the deformable particle easily experiences the fluid induced force, so the displacement change of deformable particle is

larger than the rigid particle. The figure 4-7 shows the graph about the focusing y-position of different particles at the 230 ㎛ on x-axis. The graph summarizes the displacement date of figure from 4-4. To figure 4-6. The deformability of particles and applied fluid velocity affect to the focusing y-position of particle. Under the condition of fluid velocity as 600 ㎛/s, the soft particle is distinctively focused to different position, so the soft particle can be easily separated. At the 900 ㎛/s of fluid velocity, the focusing position of rigid particle is remarkably focused to near to the initial position, so the analysis using the rigid particle could not describe the separation phenomenon in MOFF. The difference between the trajectories of rigid and deformable particles can affect to the separation result as well as difference between the focusing position of stiff and soft particle. The deformability of particle is required to describe and analyze the separation of particles.

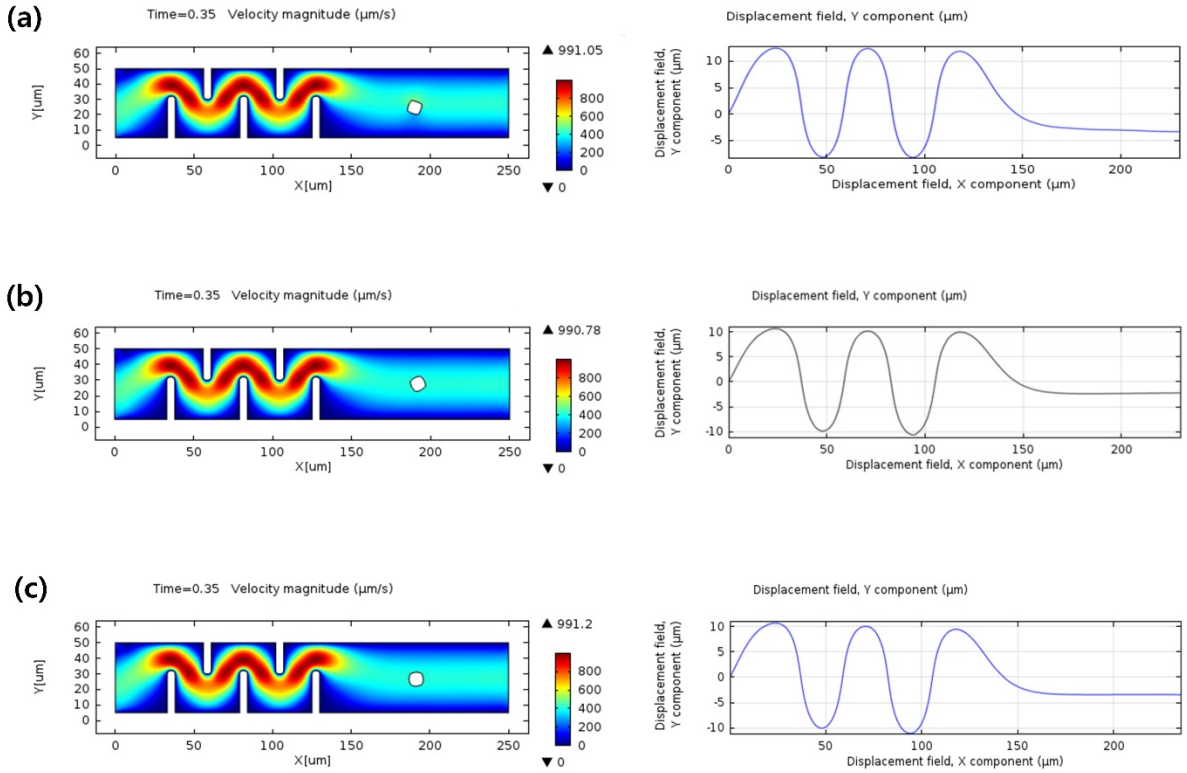

Figure 4-4. Three type of particle trajectories in the compacted MOFF model are described. The initial position of particle and the boundary condition are fixed and the inlet fluid velocity is 300 ㎛/s. At the same time as 0.35s, the positions of particles at the velocity magnitude field are close to the 200 ㎛ at x-axis. (a) The final focusing y position of rigid particle is far from the initial y component of particle and its distant is longer than other deformable particle. (b) The stiff particle is finally focused to its position that is similar to the y component of the initial position of this particle. (b) The y component of focusing position of soft particle also similar to the zero.

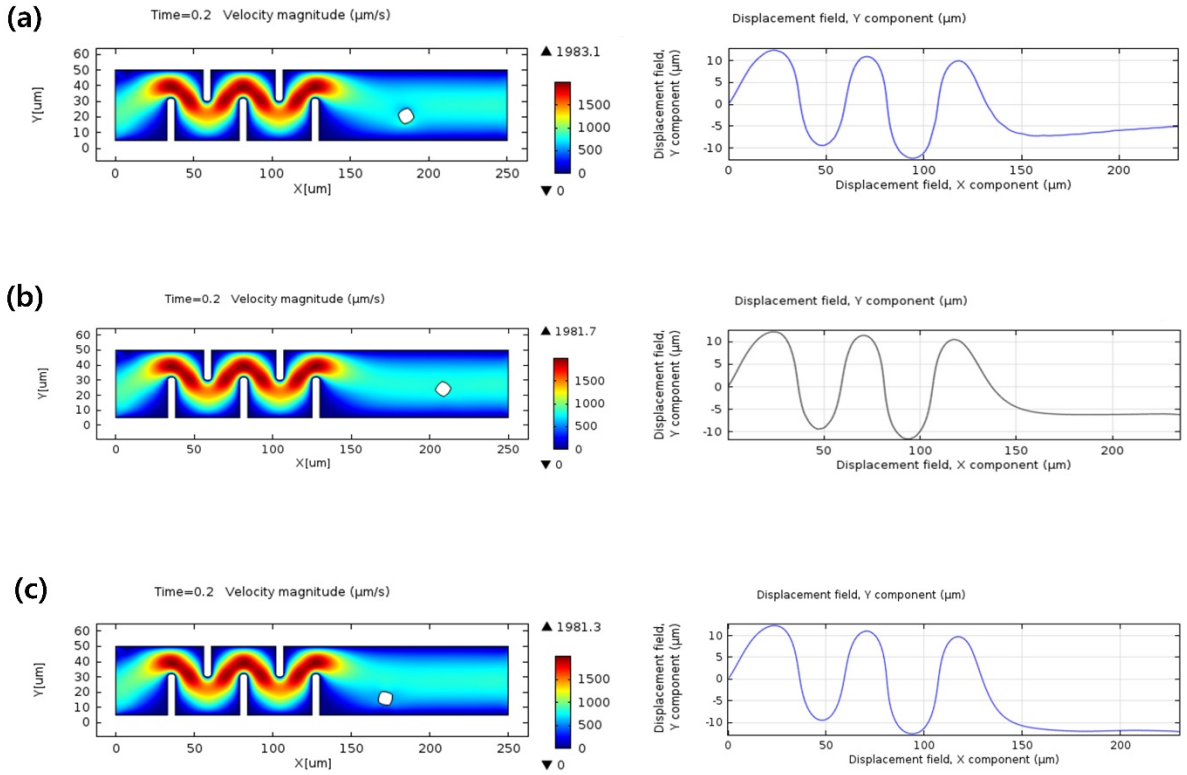

Figure 4-5. The different particle trajectories in the compacted MOFF model are described with 600 ㎛/s of inlet fluid velocity. (a) is the rigid particle, (b) is the stiff particle and (c) is the soft particle. At the same time as 0.2s, the positions of deformable particles at the velocity magnitude field are far from the 200 ㎛ at x-axis but the rigid particle only lags from the 200 ㎛ at x-axis. Three particles are focused to lower position than those of initial position. The focusing y component of different particles are close to the -5 ㎛ position, but there are slight gap between the focusing position of three particles.

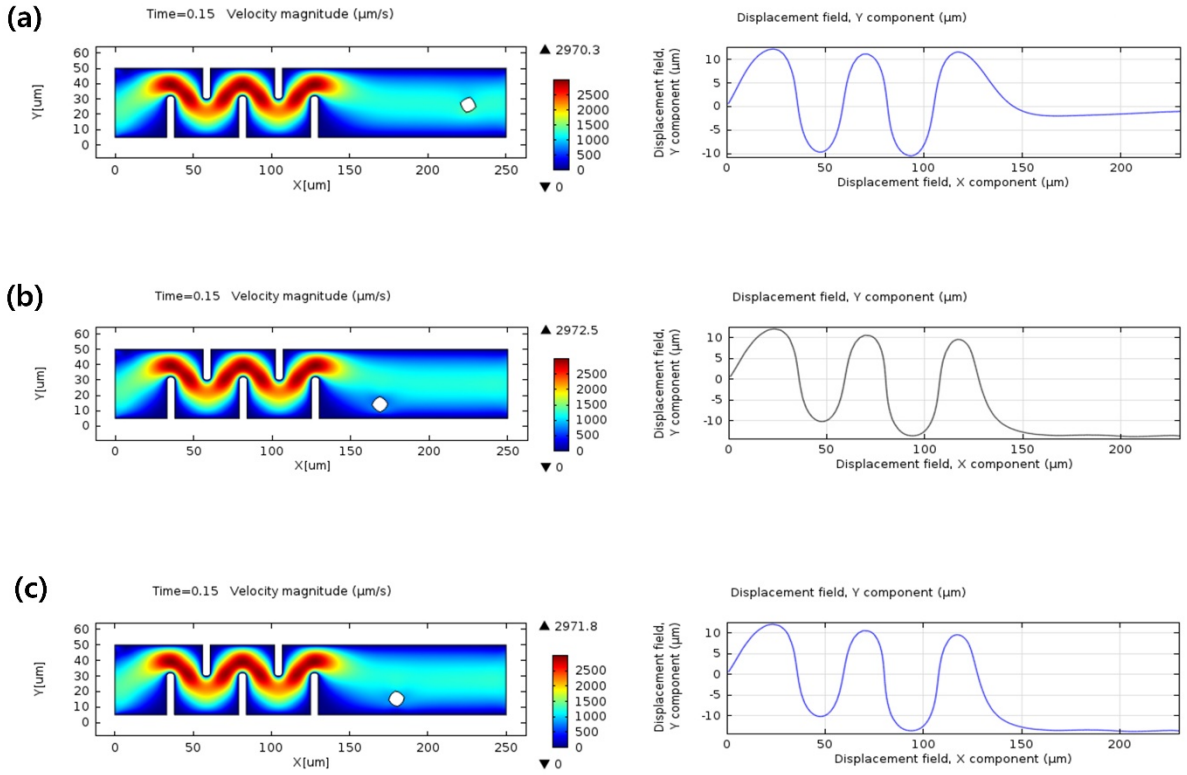

Figure 4-6. The stiff and soft particle trajectories in the compacted MOFF model are described with 900 ㎛/s of fluid velocity. (a) is the rigid particle, (b) is the stiff particle and (c) is the soft particle. At the same time as 0.15s, the positions of rigid and soft particles at the velocity magnitude field are far from the 200 ㎛ at x-axis, specially the x-position of rigid particle is the longest. The stiff particle only could not pass the 200 ㎛ at x-axis. Three particles are commonly focused to lower position from the original y component of particles. The rigid particle focusing position is close to the 0 ㎛, but the deformable particles are focused far from the 0 ㎛ and lower position near or under -10 ㎛.

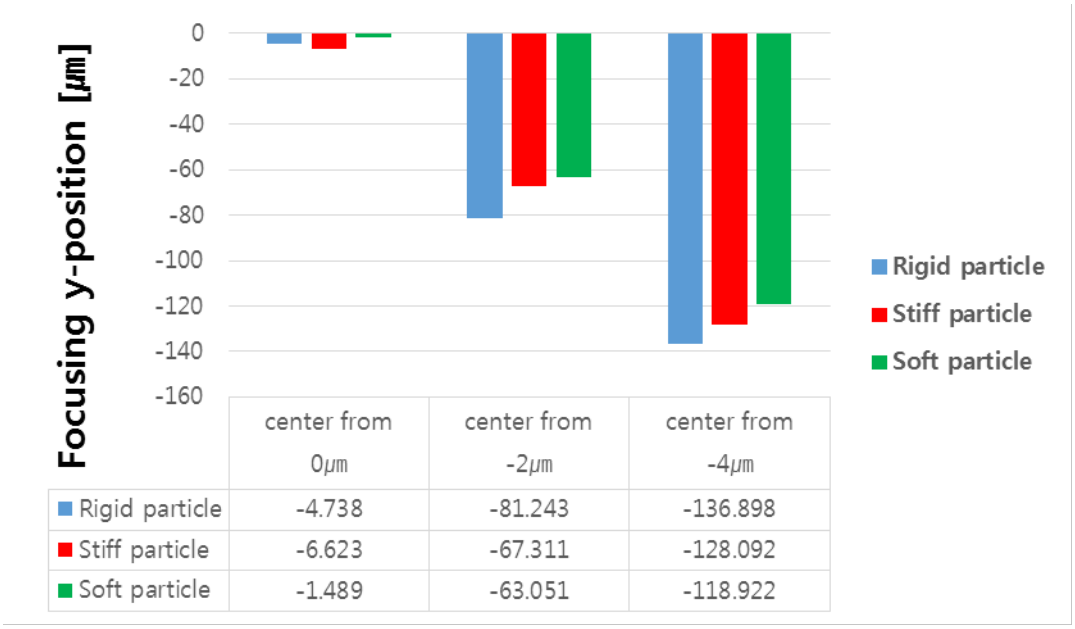

	center from 0㎛	center from -2㎛	center from -4㎛
Rigid particle	-4.738	-81.243	-136.898
Stiff particle	-6.623	-67.311	-128.092
Soft particle	-1.489	-63.051	-118.922

Figure 4-7. The graph shows a y component of final focusing position of different particles. The gap between the y component of focusing position of rigid, stiff and soft particle. Three different particles commonly travel away from the center line of microfluidic model. The y component of focusing position of each particles is different at the same fluid velocity or the increased fluid velocity as 300, 600 and 900 ㎛/s. The different particles are always focused at down position and the distance from the initial 0 ㎛ to focusing position increases along the increased fluid velocity except to the rigid particle.

3.4 Particle trajectory in ending expansion area

At the final expansion area, the final position of particles is decisive to separate the different particles. After the ending expansion area, the sample outlet for the cancer cell or blood cell are linked to collect the targeted cell. Therefore, the particle trajectory and the final focusing position are important and critical for the capture efficiency and the capture purity. So, the divided module of the ending expansion of MOFF is simulated to observe the distinct difference between the rigid particle and the different deformable particles. The particle size and the fluid condition like the inflow velocity are given as 0.85m/s, 10㎛ and the boundary condition of the model are fixed. The trajectory of the particle is simulated with different initial particle position at the start point of ending expansion area and the different deformability parameter. The displacement of three different particles is changed by the different interaction result between the fluid flowing and the several deformability parameter of particles. And the initial position of the particle at start point of ending expansion area affects to the displacement and the final focusing position of particle at the channel. The displacement of three particles describes from the 0㎛ to 800㎛ of x-axis.

3.4.1 Focusing position with different deformability

The different deformability of different particles affects the particle trajectory. Because the rigid and deformed particle, and the fluid flowing interact each other, the trajectory of particles is changed. The difference of the trajectory several particle is shown at figure 4-8. As shown figure 4-8 (a)-(c), the displacement of different particles, which are located to the center of inlet. The different particles horizontally flow and the focusing position of rigid, stiff and soft particle at the near 800㎛ are -4.7190㎛, -6.6232㎛ and -1.4897㎛, respectively. The focusing y-position of soft particle is nearest to the initial y-position, but the rigid and stiff particle are focused to lower position than initial. If all particles are located to low position than the centerline about 2㎛, the trajectories of three particles are shown at figure 4-8 (d)-(f). The particle trajectory is regular until 100㎛ of x-direction and the change of trajectory starts at the ending of contraction area. All particle moves to the down direction from the initial position and the final focusing positions are measured at the 800㎛. The final focusing y-component of three particles are -81.243㎛, -67.311㎛ and -63.051㎛, respectively. The distance from the initial y-position to focusing y-position of rigid particle is the lowest and the deformable particles are focused to upper position than the rigid particle. Figure 4-7(g)-(i) shows the displacement of three particles, when all particles are initially positioned to -4㎛ from centerline. The final focusing y-position of rigid, stiff and soft particles are -136.898㎛, -128.092㎛ and -118.922㎛, respectively. The distance from the initial position to focusing position of rigid particles are longer than the deformable particles. The different particles at the same initial position are differently focused to their focusing position. Because the deformability of particles are differently given, the trajectories between the rigid and deformable particles are different and they can be separated in the microchannel.

3.4.2 Focusing position with different initial position

In the simulation, the rigid particle and the deformable particles are initially located to the center and near center point of the contraction chamber like center, center from 2 and 4㎛. Located three different particles flow to their equilibrium position. The initial position of particle is calibrated to zero and the position of particle is calculated based on the initial position. As figure4-8., three column of displacement graphs show the trajectories of rigid, stiff and soft particle in the microchannel in order. The rigid particle displacement is described to figure 4-8(a), (d) and (g), the final focusing y-position is down-direction from the zero. The particle initial distance from the centerline increases, the distance of focusing position becomes lower than initial position. When the rigid particle initial position shifts to -2㎛ at the start point, the focusing y-position shifts to low position with 76.505㎛ of gap between the centerline and -2㎛ position. Also when the initial position shifts to -4㎛, the focusing y-position shifts to low position with 55.655㎛ of gap between -2㎛ position and -4㎛ position. Figure 4-8(b), (e) and (h) shows the stiff particle trajectory with different initial position. The gap between the result of stiff particle focusing positions, which are originally located to centerline and -2㎛ at the start area, are 60.688㎛. And this particle is firstly located to -4 ㎛, the gap between the result of particle focusing positions, which are initially located to -2㎛ and -4㎛, the gap between the focusing positions is 60.781㎛. The soft particle trajectory with different initial location is described at figure 4-8(c), (f) and (i). The gap between final focusing y-positions of soft particles, which are initially located to centerline and -2㎛ position at the starting, is 61.562㎛. The gap between final focusing y-positions of soft particles, which are initially located to- 2㎛ and -4㎛ position at the

starting, is 55.871㎛. The initial particle position at the ending expansion area affects to the particle trajectory and the final focusing y-position also changes.

The summery of different particle displacement are shown as figure 4-9. In the result of the experiment of the MOFF system, the large cell is focused to the center of microchannel. Because the equilibrium position of the cell is effected the size of the cell, the large cell is focused to the center line and the small cell is focused away from the center line. The rigid particle tends to easily get out the initial trajectory and it is focused to the distant position. The initial position of particle affects to the final focusing y-position. The small gap at the initial position generates the large gap at the focusing position. Whichever particle is initially located to centerline, the particle moves to horizontally to smaller than -10㎛. If the particle is located at the start point with distance from the centerline, the focusing position is far from the initial y-position.

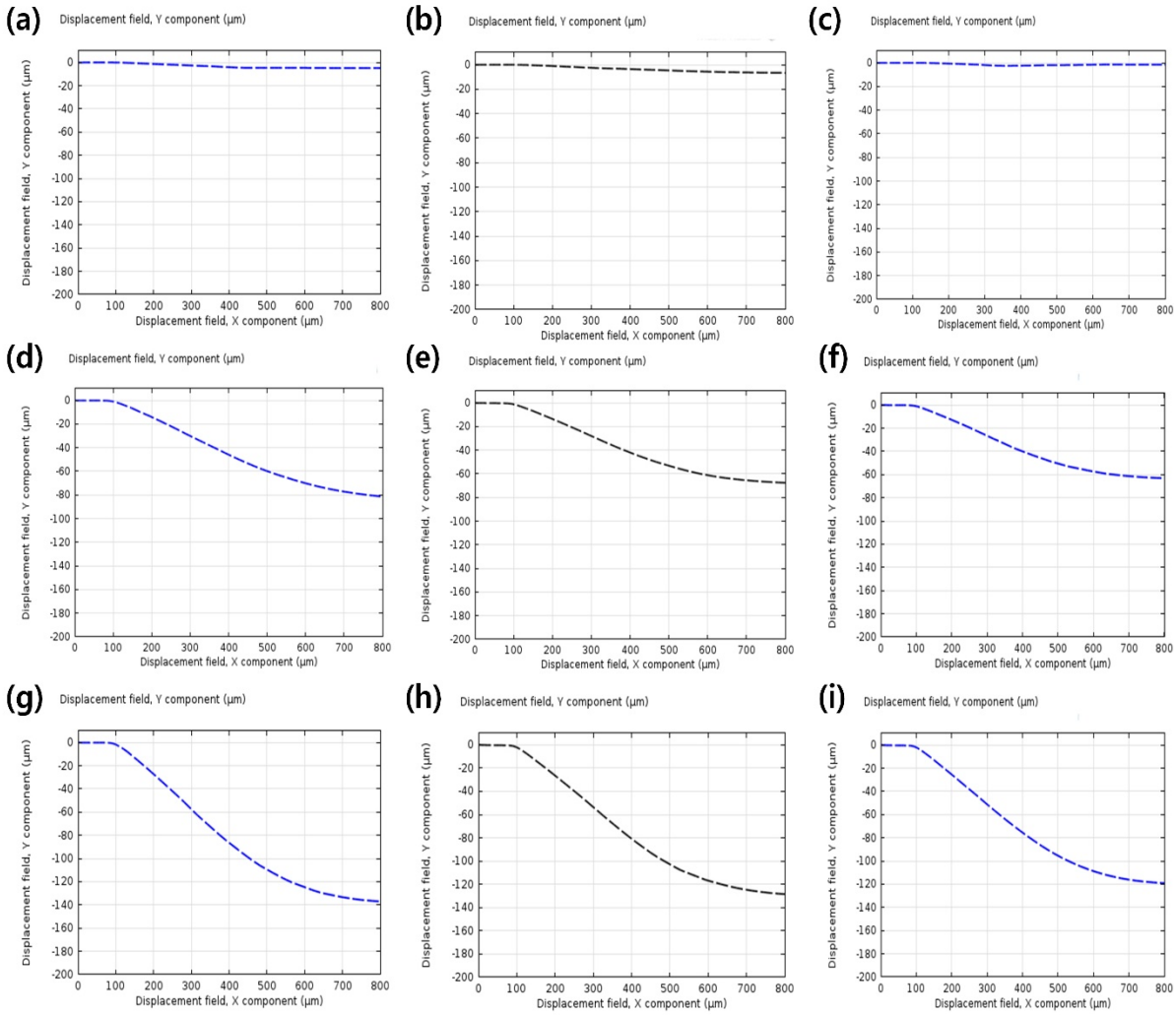

Figure 4-8. The divided expansion MOFF model and the graph of x-y displacement of different particles are shown. The length of x axis is fixed to 800 ㎛, the minimum and maximum length of y axis are fixed to -400 ㎛ and 40 ㎛. The -400 ㎛ means the half length of expansion chamber. The inflow velocity is 0.85m/s and the given original position of particles are fixed as center of inlet channel, -2 ㎛ and -4 ㎛ far from the center. The 0 ㎛ on the y axis means the particle center point. The particles are initially located at center and flow in the microchannel as (a)-(c), at -2 ㎛ from the center as (d)-(f) and at -4 ㎛ from the center as (g)-(i). The rigid particle trajectories on the center, -2 and -4 ㎛ from the center are described as (a), (d) and (g). The stiff particle trajectories on the center, -2 and -4 ㎛ from the center are described as (b), (e) and (h). The rigid particle trajectories on the center, -2 and -4 ㎛ from the center are described as (c), (f) and (i). If particles are located at center, they move

near the 0 ㎛. But, the particles, which are located beside to the center, move to lower position than the initial position. The trajectories of different particles, which are located to -2 or -4 ㎛ from the center, commonly changes after 100 ㎛, because this point is a start part of ending expansion camber of MOFF model.

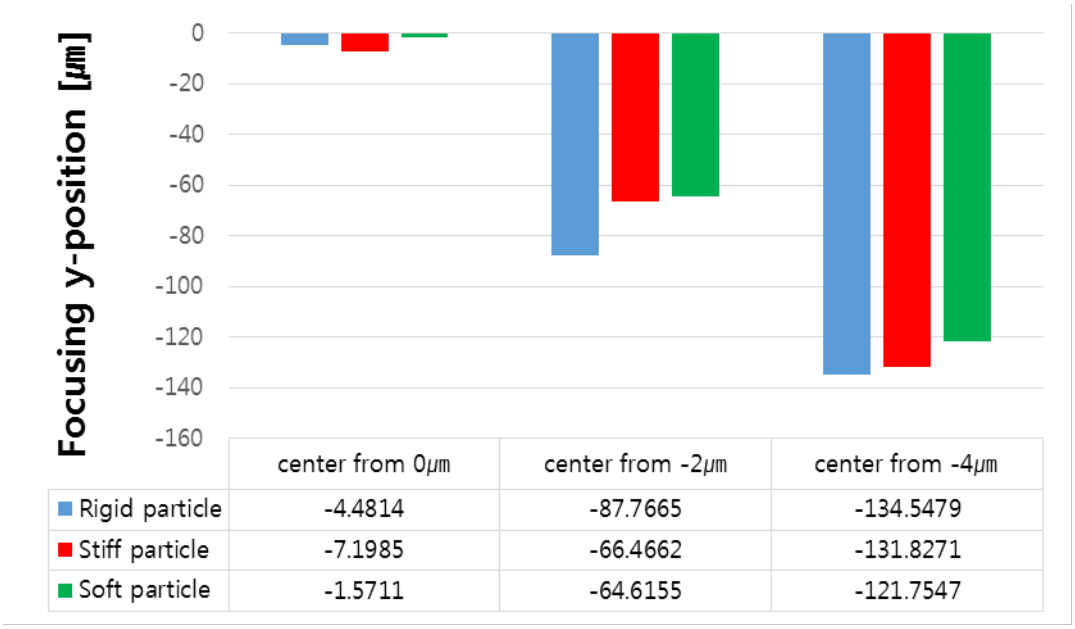

	center from 0㎛	center from -2㎛	center from -4㎛
Rigid particle	-4.4814	-87.7665	-134.5479
Stiff particle	-7.1985	-66.4662	-131.8271
Soft particle	-1.5711	-64.6155	-121.7547

Figure 4-9. The graph shows the final focusing y component of different three particle with different initial position at the start point. The particle is located three position as on the center line, far from the 2 ㎛ and 4 ㎛ position. The simulation conditions are same to those of the figure 4-8. The gap between the initial and focusing y position of three particles usually increases by effects of the different initial position. The final focusing y position between rigid particle and deformable particles are different. When the particle are originally located on the side of center, the rigid particle is focused to the far position from the centerline. But if the particle is located to center, the stiff particle is focused to the far position than the other particles. Compared between stiff and soft particles, the stiff particle tends to be focused lower position than soft particle regardless of initial position.

4. CONCLUSION

90% of the cancer related death dues to the metastasis of the cancer, not the primary caner. The cancer cell can escape from the primary cancer tissue and enter to the blood or lymphatic stream system. The cancer cell also can invade to the near organs or the remote location to attach and spread out. This cancer cell is called as the circulating tumor cell (CTC), it is a trigger of the metastasis. Therefore CTC should be detected from the whole blood and subsequently analyzed. Because CTC is derived from the primary cancer, it indicates the cancer status and the information of the cancer. By the analysis of detected CTC helps to the medical decision like a diagnosis and treatment of the cancer. Moreover analysis of CTC can be used to develop the new drug or specific biomarker since CTC has the numerous heterogeneity.

To use CTC in the medical area and the research area, the separation technology of CTC is required and this technology has been developing. The separation methods using the microfluidic system are introduced, because the microfluidic system can offer the easy handling of liquid, the low cost fabrication, the a number of replica and this system can integrate with other techniques that improve the efficiency of the device. Using the microfluidic device, the technology for separation of CTC are categorized with the specific molecule on the surface of CTC, the higher dielectric property than other blood cell, and less deformable and the large size. Among the separation method based on the physical properties, the size based isolation has a number of advantages like a non-labelling, high throughput, high capture efficiency and the less cell damage. These advantages are the key parameters to evaluate the separation method, the hydrodynamic size based isolation method concededly meets these parameters than other method. Especially the multi-orifice flow fractionation

(MOFF) system can offer the highest capture efficiency almost 100 percentages with the cancer cell lines spiked blood sample. However, the hydrodynamic size based separation has the limitation, which is the low capture purity. The capture purity is important to subsequent molecule analysis. If the undesired blood cells exist in the collected CTC outlet, these blood cells disturb the analysis and the result of the analysis is not reliable. The reason of the low capture purity is interpreted as the size overlapping between the blood cell (leukocyte) and CTC. To keep the high capture efficiency and enhance the capture purity of MOFF system, the additional approach is needed to interpret the phenomena of low capture purity. The cell deformability will be considered to analyze the low capture purity because the blood cell and CTC can deform while separation process and the deformed cells affects to the capture purity. Therefore, the rigid and deformable particle trajectories are calculated by using the COMSOL simulation tool. Moreover, the different particles are applied in the compacted MOFF model, which is designed to short the channel dimension and the calculation time. Based on the fluid flow, solid mechanics and fluid-solid interaction (FSI) governs the behavior of the particle and the fluid.

In result, the deformability parameter affects to the particle trajectory and the equilibrium position of the particle. Other condition like as fluid velocity and the initial position of the particle affects to the difference of trajectory of particle. But the deformability parameter is newly applied to interpret the phenomena of the separation in the microfluidic model and this parameter significantly affects to the simulation results. In simulation based the FSI, the particle deformability is applied to the rigid, stiff and soft particle. Despite of designed particles are same size, the particles are focused to different position. The difference between the rigid particle and deformable particles shows as the different particle trajectories and final particle focusing position. By applying the particle deformability

parameter, the deformable particle experiences different fluid induced force from the rigid particle. Especially the rigid particle has far y axial distance from the initial y-position than deformable particles at the ending expansion area. Also the stiff and soft particle focus to different position. The soft particle tends to near to the initial center area, which is the experimentally the experimental cancer cell collecting area, so the soft particle disturbs the separation boundary between the cancer and blood cell. The deformability of particle affects to the separation position and the separation result shows the reason of the low capture purity.

In previous researches for separation between the tumor cell and the normal blood cell analyzed and calculated the isolation phenomenon with considering to both of two cells as rigid particles. The analysis with rigid particle could not describe the separation phenomenon in the microchannel. The deformability of cell is not reflected, so the analysis could not describe the real experimental separation result. Therefore, the separation between the soft particle and stiff particle in the final collect channel is difficult. Also the reason of the low capture purity of MOFF system is not only the size overlapping between the soft cells (leukocytes) and the stiff cells (CTCs), but also the different deformability properties of different cells. The additional approach for interpreting the limitation of the size based separation technology is required to analyze the experiment result and to solve the problem like as low capture purity. To accurate and realistic analysis of the separation phenomenon in the microchannel and the capture purity, the deformability property of applied particle should be considered. Based on this simulation results, the method for increasing the shear force acting on the deformable particle should be applied.

REFERENCE

1. *Cancer Fact sheet N°297.* World Health Organization, 2014.

2. Folkman, J., *Tumor angiogenesis: therapeutic implications.* N Engl J Med, 1971. 285(21): p. 1182-6.

3. Nishida, N., et al., *Angiogenesis in cancer.* Vascular health and risk management, 2006. 2(3): p. 213.

4. Gupta, G.P. and J. Massagué, *Cancer metastasis: building a framework.* Cell, 2006. 127(4): p. 679-695.

5. LICHSTEIN, P.R., *3 The Medical Interview.* Clinical methods: The history, physical, and laboratory examinations, 1990: p. 29.

6. Reiser, D.E. and A.K. Schroder, *Patient interviewing: the human dimension*. 1980: Williams & Wilkins Company.

7. Henschke, C.I., et al., *Survival of patients with stage I lung cancer detected on CT screening.* The New England journal of medicine, 2006. 355(17): p. 1763-1771.

8. Lehman, C.D., et al., *MRI evaluation of the contralateral breast in women with recently diagnosed breast cancer.* New England Journal of Medicine, 2007. 356(13): p. 1295-1303.

9. Timmerman, D., et al., *Simple ultrasound-based rules for the diagnosis of ovarian cancer.* Ultrasound in obstetrics & gynecology, 2008. 31(6): p. 681-690.

10. Weissleder, R., *Molecular imaging in cancer.* Science, 2006. 312(5777): p. 1168-1171.

11. Sollier, E., et al., *Size-selective collection of circulating tumor cells using Vortex technology.* Lab on a Chip, 2014. 14(1): p. 63-77.

12. Thomson, K.R. and D. Varma, *Safe use of radiographic contrast media.* Australian Prescriber, 2010. 33(1): p. 19-22.

13. Yu, M., et al., *Circulating tumor cells: approaches to isolation and characterization.* The Journal of cell biology, 2011. 192(3): p. 373-382.

14. Diamantis, A., E. Magiorkinis, and H. Koutselini, *Fine-needle aspiration (FNA) biopsy: historical aspects.* Folia Histochemica et Cytobiologica, 2009. 47(2): p. 191-197.

15. Frable, W.J., *Fine-needle aspiration biopsy: a review.* Human pathology, 1983. 14(1): p. 9-28.

16. Kline, T.S. and H.F. Frierson Jr, *Handbook of Fine Needle Aspiration Biopsy Cytology.* The American Journal of Surgical Pathology, 1988. 12(12): p. 970.

17. Sheng, W., et al., *Capture, release and culture of circulating tumor cells from pancreatic cancer patients using an enhanced mixing chip.* Lab on a Chip, 2014. 14(1): p. 89-98.

18. Alix-Panabières, C. and K. Pantel, *Circulating tumor cells: liquid biopsy of cancer.* Clinical chemistry, 2013. 59(1): p. 110-118.

19. Pantel, K. and C. Alix-Panabières, *Circulating tumour cells in cancer patients: challenges and perspectives.* Trends in molecular medicine, 2010. 16(9): p. 398-406.

20. Nagrath, S., et al., *Isolation of rare circulating tumour cells in cancer patients by microchip technology.* Nature, 2007. 450(7173): p. 1235-1239.

21. Ashworth, T., *A case of cancer in which cells similar to those in the tumours were seen in the blood after death.* Aust Med J, 1869. 14(3): p. 146-149.

22. Zheng, X., et al., *A high-performance microsystem for isolating circulating tumor cells.* Lab on a Chip, 2011. 11(19): p. 3269-3276.

23. Tan, S.J., et al., *Microdevice for the isolation and enumeration of cancer cells from blood.* Biomedical microdevices, 2009. 11(4): p. 883-892.

24. Wiedswang, G. and B. Naume, *Can detection of circulating tumor cells in peripheral blood provide prognostic data in breast cancer?* Nature Clinical Practice Oncology, 2007. 4(3): p. 154-155.

25. Mocellin, S., et al., *The prognostic value of circulating tumor cells in patients with melanoma: a systematic review and meta-analysis*. Clinical Cancer Research, 2006. 12(15): p. 4605-4613.

26. Cristofanilli, M., et al., *Circulating tumor cells, disease progression, and survival in metastatic breast cancer.* New England Journal of Medicine, 2004. 351(8): p. 781-791.

27. van de Stolpe, A., et al., *Circulating tumor cell isolation and diagnostics: toward routine clinical use.* Cancer research, 2011. 71(18): p. 5955-5960.

28. Powell, A.A., et al., *Single cell profiling of circulating tumor cells: transcriptional*

heterogeneity and diversity from breast cancer cell lines. PloS one, 2012. 7(5): p. e33788.

29. Gupta, G., et al. *Identifying site-specific metastasis genes and functions*. in *Cold Spring Harbor symposia on quantitative biology*. 2005. Cold Spring Harbor Laboratory Press.

30. Allard, W.J., et al., *Tumor cells circulate in the peripheral blood of all major carcinomas but not in healthy subjects or patients with nonmalignant diseases.* Clinical Cancer Research, 2004. 10(20): p. 6897-6904.

31. Sun, Y.-F., et al., *Circulating tumor cells: advances in detection methods, biological issues, and clinical relevance.* Journal of cancer research and clinical oncology, 2011. 137(8): p. 1151-1173.

32. Hyun, K.-A. and H.-I. Jung, *Advances and critical concerns with the microfluidic enrichments of circulating tumor cells.* Lab on a Chip, 2014. 14(1): p. 45-56.

33. Jin, C., et al., *Technologies for label-free separation of circulating tumor cells: from historical foundations to recent developments.* Lab on a Chip, 2014. 14(1): p. 32-44.

34. Attard, G. and J.S. de Bono, *Utilizing circulating tumor cells: challenges and pitfalls.* Current opinion in genetics & development, 2011. 21(1): p. 50-58.

35. den Toonder, J., *Circulating tumor cells: the Grand Challenge*. Lab on a chip, 2011. 11(3): p. 375-377.

36. Paris, P.L., et al., *Functional phenotyping and genotyping of circulating tumor cells from patients with castration resistant prostate cancer.* Cancer letters, 2009. 277(2): p. 164-173.

37. Kim, M.-Y., et al., *Tumor self-seeding by circulating cancer cells.* Cell, 2009. 139(7): p. 1315-1326.

38. Comen, E., L. Norton, and J. Massague, *Clinical implications of cancer self-seeding*. Nature reviews Clinical oncology, 2011. 8(6): p. 369-377.

39. Niikura, N., et al., *Loss of human epidermal growth factor receptor 2 (HER2) expression in metastatic sites of HER2-overexpressing primary breast tumors.* Journal of Clinical Oncology, 2012. 30(6): p. 593-599.

40. Jackson, E.L. and H. Lu, *Advances in microfluidic cell separation and manipulation.* Current opinion in chemical engineering, 2013. 2(4): p. 398-404.

41. Kang, J.H. and J.-K. Park, *Cell separation technology.* Yeast, 2004. 90.

42. Andersson, H. and A. Van den Berg, *Microfluidic devices for cellomics: a review.* Sensors and Actuators B: Chemical, 2003. 92(3): p. 315-325.

43. Salieb-Beugelaar, G.B., et al., *Latest developments in microfluidic cell biology and analysis systems.* Analytical chemistry, 2010. 82(12): p. 4848-4864.

44. El-Ali, J., P.K. Sorger, and K.F. Jensen, *Cells on chips.* Nature, 2006. 442(7101): p. 403-411.

45. Königsberg, R., et al., *Detection of EpCAM positive and negative circulating tumor cells in metastatic breast cancer patients.* Acta oncologica, 2011. 50(5): p. 700-710.

46. Maheswaran, S. and D.A. Haber, *Circulating tumor cells: a window into cancer biology and metastasis.* Current opinion in genetics & development, 2010. 20(1): p. 96-99.

47. Patriarca, C., et al., *Epithelial cell adhesion molecule expression (CD326) in cancer: a short review.* Cancer treatment reviews, 2012. 38(1): p. 68-75.

48. Earhart, C.M., et al., *Isolation and mutational analysis of circulating tumor cells from lung cancer patients with magnetic sifters and biochips.* Lab on a Chip, 2014. 14(1): p. 78-88.

49. Andreopoulou, E., et al., *Comparison of assay methods for detection of circulating tumor cells in metastatic breast cancer: AdnaGen AdnaTest BreastCancer Select/Detect™ versus Veridex CellSearch™ system.* International Journal of Cancer, 2012. 130(7): p. 1590-1597.

50. Miller, M.C., G.V. Doyle, and L.W. Terstappen, *Significance of circulating tumor cells detected by the CellSearch system in patients with metastatic breast colorectal and prostate cancer.* Journal of oncology, 2009. 2010.

51. Harouaka, R.A., M. Nisic, and S.-Y. Zheng, *Circulating tumor cell enrichment based on physical properties.* Journal of laboratory automation, 2013. 18(6): p. 455-468.

52. Hyun, K.-A., T.Y. Lee, and H.-I. Jung, *Negative enrichment of circulating tumor cells using a geometrically activated surface interaction chip.* Analytical chemistry, 2013. 85(9): p. 4439-4445.

53. Gascoyne, P.R., et al., *Dielectrophoretic separation of cancer cells from blood.* Industry Applications, IEEE Transactions on, 1997. 33(3): p. 670-678.

54. Díaz, R. and S. Payen, *Biological cell separation using dielectrophoresis in a microfluidic*

device. University of California, Berkeley, Bio and Thermal Engineering Laboratory EECS. 245.

55. Gascoyne, P., et al., *Dielectrophoretic separation of mammalian cells studied by computerized image analysis.* Measurement Science and Technology, 1992. 3(5): p. 439.

56. Pethig, R., et al., *Dielectrophoresis: a review of applications for stem cell research.* BioMed Research International, 2010. 2010.

57. Gascoyne, P.R., et al., *Isolation of rare cells from cell mixtures by dielectrophoresis.* Electrophoresis, 2009. 30(8): p. 1388-1398.

58. Huang, Y., et al., *Membrane changes associated with the temperature-sensitive P85< sup> gag-mos</sup>-dependent transformation of rat kidney cells as determined by dielectrophoresis and electrorotation.* Biochimica et Biophysica Acta (BBA)-Biomembranes, 1996. 1282(1): p. 76-84.

59. Gascoyne, P., et al., *Dielectrophoretic detection of changes in erythrocyte membranes following malarial infection.* Biochimica et Biophysica Acta (BBA)-Biomembranes, 1997. 1323(2): p. 240-252.

60. Chan, K.L., et al., *Electrorotation of liposomes: verification of dielectric multi-shell model for cells.* Biochimica et Biophysica Acta (BBA)-Lipids and Lipid Metabolism, 1997. 1349(2): p. 182-196.

61. Yang, J., et al., *Dielectric properties of human leukocyte subpopulations determined by electrorotation as a cell separation criterion.* Biophysical Journal, 1999. 76(6): p. 3307-3314.

62. Diamandis, E.P., *Tumor markers: physiology, pathobiology, technology, and clinical applications*. 2002: Amer. Assoc. for Clinical Chemistry.

63. Huang, Y., et al., *The removal of human breast cancer cells from hematopoietic CD34+ stem cells by dielectrophoretic field-flow-fractionation.* Journal of hematotherapy & stem cell research, 1999. 8(5): p. 481-490.

64. Becker, F.F., et al., *Separation of human breast cancer cells from blood by differential dielectric affinity.* Proceedings of the National Academy of Sciences, 1995. 92(3): p. 860-864.

65. Das, C.M., et al., *Dielectrophoretic segregation of different human cell types on microscope slides.* Analytical chemistry, 2005. 77(9): p. 2708-2719.

66. Hyun, K.A. and H.I. Jung, *Microfluidic devices for the isolation of circulating rare cells: A focus on affinity-based, dielectrophoresis, and hydrophoresis.* Electrophoresis, 2013. 34(7): p. 1028-1041.

67. Suresh, S., et al., *Connections between single-cell biomechanics and human disease states: gastrointestinal cancer and malaria.* Acta biomaterialia, 2005. 1(1): p. 15-30.

68. Suwanarusk, R., et al., *The deformability of red blood cells parasitized by Plasmodium falciparum and P. vivax.* Journal of Infectious Diseases, 2004. 189(2): p. 190-194.

69. Suresh, S., *Biomechanics and biophysics of cancer cells.* Acta Materialia, 2007. 55(12): p. 3989-4014.

70. Lincoln, B., et al., *Deformability-based flow cytometry.* Cytometry Part A, 2004. 59(2): p. 203-209.

71. Guck, J., et al., *Optical deformability as an inherent cell marker for testing malignant transformation and metastatic competence.* Biophysical journal, 2005. 88(5): p. 3689-3698.

72. Cross, S.E., et al., *Nanomechanical analysis of cells from cancer patients.* Nature nanotechnology, 2007. 2(12): p. 780-783.

73. Mohandas, N. and S. Shohet, *Control of red cell deformability and shape.* Current topics in hematology, 1978. 1: p. 71.

74. Brandao, M., et al., *Optical tweezers for measuring red blood cell elasticity: application to the study of drug response in sickle cell disease.* European journal of haematology, 2003. 70(4): p. 207-211.

75. Hur, S.C., et al., *Deformability-based cell classification and enrichment using inertial microfluidics.* Lab on a Chip, 2011. 11(5): p. 912-920.

76. Preira, P., et al., *Passive circulating cell sorting by deformability using a microfluidic gradual filter.* Lab on a Chip, 2013. 13(1): p. 161-170.

77. Lekka, M., et al., *Elasticity of normal and cancerous human bladder cells studied by scanning force microscopy.* European Biophysics Journal, 1999. 28(4): p. 312-316.

78. Weitz, J., et al., *Dissemination of tumor cells in patients undergoing surgery for colorectal cancer.* Clinical cancer research, 1998. 4(2): p. 343-348.

79. Kuo, J.S., et al., *Deformability considerations in filtration of biological cells.* Lab on a Chip, 2010. 10(7): p. 837-842.

80. McFaul, S.M., B.K. Lin, and H. Ma, *Cell separation based on size and deformability using microfluidic funnel ratchets.* Lab on a chip, 2012. 12(13): p. 2369-2376.

81. Mohamed, H., et al., *Isolation of tumor cells using size and deformation.* Journal of Chromatography A, 2009. 1216(47): p. 8289-8295.

82. Zhang, W., et al., *Microfluidics separation reveals the stem-cell–like deformability of tumor-initiating cells.* Proceedings of the National Academy of Sciences, 2012. 109(46): p. 18707-18712.

83. Chen, Y., et al., *Rare cell isolation and analysis in microfluidics.* Lab on a Chip, 2014. 14(4): p. 626-645.

84. Hou, H.W., et al., *Microfluidic devices for blood fractionation.* Micromachines, 2011. 2(3): p. 319-343.

85. Karimi, A., S. Yazdi, and A. Ardekani, *Hydrodynamic mechanisms of cell and particle trapping in microfluidics.* Biomicrofluidics, 2013. 7(2): p. 021501.

86. Zheng, S., et al., *Membrane microfilter device for selective capture, electrolysis and genomic analysis of human circulating tumor cells.* Journal of Chromatography A, 2007. 1162(2): p. 154-161.

87. Wheater, P.R., H.G. Burkitt, and V.G. Daniels, *Functional histology. A text and colour atlas*. 1979: Churchill Livingstone, 23 Ravelston Terrace, Edinburgh, EH4 3TL.

88. Handin, R.I., S.E. Lux, and T.P. Stossel, *Blood: principles and practice of hematology*. Vol. 1. 2003: Lippincott Williams & Wilkins.

89. Xin, H., et al., *Photothermal trapping of dielectric particles by optical fiber-ring.* Optics express, 2011. 19(3): p. 2711-2719.

90. Tanaka, M., H. Monjushiro, and H. Watarai, *Laser photophoretic migration with periodic expansion-contraction motion of photo-absorbing microemulsion droplets in water.* Langmuir, 2004. 20(25): p. 10791-10797.

91. Soong, C., et al., *Theoretical analysis for photophoresis of a microscale hydrophobic particle in liquids.* Optics express, 2010. 18(3): p. 2168-2182.

92. Lei, H., Y. Zhang, and B. Li, *Particle separation in fluidic flow by optical fiber.* Optics express, 2012. 20(2): p. 1292-1300.

93. Lei, H., et al., *Photophoretic assembly and migration of dielectric particles and Escherichia coli in liquids using a subwavelength diameter optical fiber.* Lab on a Chip, 2011. 11(13): p. 2241-2246.

94. Park, J.-S. and H.-I. Jung, *Multiorifice flow fractionation: continuous size-based separation of microspheres using a series of contraction/expansion microchannels.* Analytical chemistry, 2009. 81(20): p. 8280-8288.

95. Park, J.-S., S.-H. Song, and H.-I. Jung, *Continuous focusing of microparticles using inertial lift force and vorticity via multi-orifice microfluidic channels.* Lab on a Chip, 2009. 9(7): p. 939-948.

96. Kim, M.S., et al., *SSA-MOA: a novel CTC isolation platform using selective size amplification (SSA) and a multi-obstacle architecture (MOA) filter.* Lab on a Chip, 2012. 12(16): p. 2874-2880.

97. Park, J.-M., et al., *Highly efficient assay of circulating tumor cells by selective sedimentation with a density gradient medium and microfiltration from whole blood.* Analytical chemistry, 2012. 84(17): p. 7400-7407.

98. Jin, C., *Microfluidic device for continuous deformability based separation of circulating tumor cells.* Master Thesis, 2014. THE UNIVERSITY OF BRITISH COLUMBIA (Vancouver): p. 71 pages.

99. Matas, J., J. Morris, and E. Guazzelli, *Lateral forces on a sphere.* Oil & gas science and technology, 2004. 59(1): p. 59-70.

100. Asmolov, E.S., *The inertial lift on a spherical particle in a plane Poiseuille flow at large channel Reynolds number.* Journal of Fluid Mechanics, 1999. 381: p. 63-87.

101. Bhagat, A.A.S., S.S. Kuntaegowdanahalli, and I. Papautsky, *Inertial microfluidics for continuous particle filtration and extraction.* Microfluidics and nanofluidics, 2009. 7(2): p. 217-226.

102. Saffman, P., *The lift on a small sphere in a slow shear flow.* Journal of Fluid Mechanics, 1965. 22(02): p. 385-400.

103. Zeng, L., S. Balachandar, and P. Fischer, *Wall-induced forces on a rigid sphere at finite*

Reynolds number. Journal of Fluid Mechanics, 2005. 536: p. 1-25.

104. Gotoh, K., *Migration of a neutrally buoyant particle in Poiseuille flow: a possible explanation.* 1970.

105. Feng, J., H. Hu, and D. Joseph, *Direct simulation of initial value problems for the motion of solid bodies in a Newtonian fluid. Part 2. Couette and Poiseuille flows.* Journal of Fluid Mechanics, 1994. 277(271): p. 271-301.

106. Matas, J.-P., J.F. Morris, and É. Guazzelli, *Inertial migration of rigid spherical particles in Poiseuille flow.* Journal of Fluid Mechanics, 2004. 515: p. 171-195.

107. Segre, G. and A. Silberberg, *Behaviour of macroscopic rigid spheres in Poiseuille flow Part 2. Experimental results and interpretation.* Journal of Fluid Mechanics, 1962. 14(01): p. 136-157.

108. Wu, Z., et al., *Soft inertial microfluidics for high throughput separation of bacteria from human blood cells.* Lab on a Chip, 2009. 9(9): p. 1193-1199.

109. Squires, T.M. and S.R. Quake, *Microfluidics: Fluid physics at the nanoliter scale.* Reviews of modern physics, 2005. 77(3): p. 977.

110. Moon, H.-S., et al., *Continuous separation of breast cancer cells from blood samples using multi-orifice flow fractionation (MOFF) and dielectrophoresis (DEP).* Lab on a Chip, 2011. 11(6): p. 1118-1125.

111. Sim, T.S., et al., *Multistage-multiorifice flow fractionation (MS-MOFF): continuous size-based separation of microspheres using multiple series of contraction/expansion microchannels.* Lab on a Chip, 2011. 11(1): p. 93-99.

112. Moon, H.-S., et al., *Continual collection and re-separation of circulating tumor cells from blood using multi-stage multi-orifice flow fractionation.* Biomicrofluidics, 2013. 7(1): p. 014105.

113. Hyun, K.-A., et al., *Microfluidic flow fractionation device for label-free isolation of circulating tumor cells (CTCs) from breast cancer patients.* Biosensors and Bioelectronics, 2013. 40(1): p. 206-212.

114. Huang, L.R., et al., *Continuous particle separation through deterministic lateral displacement.* Science, 2004. 304(5673): p. 987-990.

115. Inglis, D.W., et al., *Critical particle size for fractionation by deterministic lateral displacement.* Lab on a Chip, 2006. 6(5): p. 655-658.

116. Green, J.V., M. Radisic, and S.K. Murthy, *Deterministic lateral displacement as a means to enrich large cells for tissue engineering.* Analytical chemistry, 2009. 81(21): p. 9178-9182.

117. Loutherback, K., et al., *Deterministic separation of cancer cells from blood at 10 mL/min.* AIP advances, 2012. 2(4).

118. Vanka, S., G. Luo, and C. Winkler, *Numerical study of scalar mixing in curved channels at low Reynolds numbers.* AIChE journal, 2004. 50(10): p. 2359-2368.

119. Dean, W., *XVI. Note on the motion of fluid in a curved pipe.* The London, Edinburgh, and Dublin Philosophical Magazine and Journal of Science, 1927. 4(20): p. 208-223.

120. Berger, S., L. Talbot, and L. Yao, *Flow in curved pipes.* Annual review of fluid mechanics, 1983. 15(1): p. 461-512.

121. Sudarsan, A.P. and V.M. Ugaz, *Fluid mixing in planar spiral microchannels.* Lab on a Chip, 2006. 6(1): p. 74-82.

122. Yamaguchi, Y., et al., *3-D simulation and visualization of laminar flow in a microchannel with hair-pin curves.* AIChE journal, 2004. 50(7): p. 1530-1535.

123. Yamaguchi, Y., et al., *Interface configuration of the two layered laminar flow in a curved microchannel.* Chemical engineering journal, 2004. 101(1): p. 367-372.

124. Therriault, D., S.R. White, and J.A. Lewis, *Chaotic mixing in three-dimensional microvascular networks fabricated by direct-write assembly.* Nature Materials, 2003. 2(4): p. 265-271.

125. Bhagat, A.A.S., S.S. Kuntaegowdanahalli, and I. Papautsky, *Continuous particle separation in spiral microchannels using dean flows and differential migration.* Lab on a Chip, 2008. 8(11): p. 1906-1914.

126. Ookawara, S., et al., *Feasibility study on concentration of slurry and classification of contained particles by microchannel.* Chemical Engineering Journal, 2004. 101(1): p. 171-178.

127. Ookawara, S., D. Street, and K. Ogawa, *Numerical study on development of particle concentration profiles in a curved microchannel.* Chemical Engineering Science, 2006. 61(11): p. 3714-3724.

128. Di Carlo, D., et al., *Continuous inertial focusing, ordering, and separation of particles in microchannels.* Proceedings of the National Academy of Sciences, 2007. 104(48): p. 18892-18897.

129. Hou, H.W., et al., *Isolation and retrieval of circulating tumor cells using centrifugal forces.* Scientific reports, 2013. 3.

130. JunáHuang, T., *Probing circulating tumor cells in microfluidics.* Lab on a chip, 2013. 13(4): p. 602-609.

131. Bruus, H., *Theoretical Microfluidics. 2008*. New York: Oxford University Press.

132. Xu, X., Z. Li, and A. Nehorai, *Finite element simulations of hydrodynamic trapping in microfluidic particle-trap array systems.* Biomicrofluidics, 2013. 7(5): p. 054108.

133. Kleppner, D. and R. Kolenkow, *An introduction to mechanics*. 2013: Cambridge University Press.

134. Bower, A.F., *Applied mechanics of solids*. 2011: CRC press.

135. Irgens, F., *Continuum mechanics*. 2008: Springer.

136. Slaughter, W.S., *The linearized theory of elasticity*. 2002: Springer.

137. Souli, M., A. Ouahsine, and L. Lewin, *ALE formulation for fluid–structure interaction problems.* Computer methods in applied mechanics and engineering, 2000. 190(5): p. 659-675.

요 약 문

마이크로플루이딕을 기반으로 하는 순환 암세포 분리 순도의 증대를 목적으로 하는 COMSOL 시뮬레이션을 이용한 새로운 접근

본 논문은 마이크로플루이딕 기반의 순환 암세포 분리에서 그 효율 및 분별 순도를 증대시키기 위하여 COMSOL 시뮬레이션을 통해 새로운 접근법을 다룬다. 순환암세포는 인체 내의 암으로부터 파생되어 혈관이나 림프선을 따라 온 몸을 순환하는 암세포로, 암의 현재 상태 및 암에 대한 정보를 가지고 있는 정보처로 여겨진다. 순환 암세포의 분리와 분리된 순환 암세포의 분자분석으로 인해 진단, 치료, 새로운 약물의 발달 및 바이오 마커의 발견을 수행할 수 있다. 마이크로플루이딕을 기반으로 하는 분리 기술은 쉽게 혈액 샘플을 다룰 수 있으며 낮은 가격의 공정 및 광학적인 시스템이나 전기적인 시스템과의 통합이 가능하여 그 효율이 증가 할 수 있기 때문에 계속적으로 발달하고 있다. 그 중 세포의 크기 차이를 기반으로 하는 유체역학적인 분리 방법 중 특히 multi-orifice flow fractionation (MOFF)는 순환 암세포를 100%에 가깝게 분리해 낼 수 있지만 분리된 샘플에서 순환 암세포의 순도는 거의 0%에 가깝다. 순도가 아주 낮은 이유는 혈액 내 백혈구의 크기 범위와 순환 암세포의 크기 범위가 일치하기 때문에, 크기가 암세포와 비슷하거나 같은 백혈구는 같은 곳으로 집중되어 분리되기 때문에 암세포 분리 순도에 영향을 미친다. 그러나 이러한 관점은 낮은 분리 순도의 현상을 이해하기에는 부족하며, 추가적인 관점으로 해석해야 한다. 추가적인 관점으로 유체 역학적인 분리 중에 발생하는 세포의 변형성을 고려해야 할 필요가 있다. COMSOL 시뮬레이션을 기반으로 마이크로플루이딕 모델링을 하여 세포의 변형성을 암세포 모델과 혈액세포 모델에 인가하였을 때, 암세포 분리의 순도에 세포 변형성의 영향에 대해 연구를 수행하였다. 그 결과 세포의 변형성으로 인하여 비교적 변형 특성이 작은 암세포는 본래의 집중되어야 하는 지점보다 벗어나 집중되고, 변형 특성이 큰 백혈구가 오히려 암세포의 집중 지점으로 모이기 때문에 분류된 샘플의 순도가 낮아지게 된다. 때문에 세포 변형성으로 인한 순도 감소의 문제점을 해결하기 위해서는 세포의 변형성이 고려되어야 하며, 분리 순도를 높이기 위해서 세포의 크기뿐만 아니라 세포의 변형성의 차이를 증가시키는 마이크로플루이딕 기술이 제안되어야 한다.

핵심어: 순환 암세포, 마이크로플루이딕, 세포 변형성, COMSOL 시뮬레이션